# Multi-wavelength polarimetric study towards the open cluster NGC 1893

C. Eswaraiah,  $^{1\star}$  A. K. Pandey,  $^1$  G. Maheswar,  $^1$  Biman J. Medhi,  $^1$ 

J. C. Pandey<sup>1</sup>, D. K. Ojha<sup>2</sup> and W. P. Chen<sup>3</sup>

<sup>1</sup> Aryabhatta Research Institute of Observational Sciences, Manora Peak, Nainital 263129, India

Accepted ———,	Received ———	-∙ in	original	form	
Accepted ———,	rtecerveu —	-, 111	Original	101111	

#### ABSTRACT

We present multi-wavelength linear polarimetric observations for 44 stars of the NGC 1893 young open cluster region along with V-band polarimetric observations of stars of other four open clusters located between  $l \sim 160^{\circ}$ to 175°. We found evidence for the presence of two dust layers located at a distance of  $\sim 170$  pc and  $\sim 360$  pc. The dust layers produce a polarization  $P_V \sim 2.2\%$ . It is evident from the clusters studied in the present work that, in the Galactic longitude range  $l \sim 160^{\circ}$  to 175° and within the Galactic plane ( $|b|<2^{\circ}$ ), the polarization angles remain almost constant, with a mean  $\sim 163^{\circ}$ and a dispersion of 6°. The small dispersion in polarization angle could be due to the presence of uniform dust layer beyond 1 kpc. Present observations reveal that in case of NGC 1893, the foreground two dust layers, in addition to the intracluster medium, seems to be responsible for the polarization effects. It is also found that towards the direction of NGC 1893, the dust layer that exists between 2-3 kpc has a negligible contribution towards the total observed polarization. The weighted mean for percentage of polarization  $(P_{max})$  and the wavelength at maximum polarization ( $\lambda_{max}$ ) are found to be  $2.59 \pm 0.02\%$ and  $0.55 \pm 0.01~\mu m$  respectively. The estimated mean value of  $\lambda_{max}$  indicates that the average size of the dust grains within the cluster is similar to that in the general interstellar medium. The spatial variation of the polarization is found to decrease towards the outer region of the cluster. In the present work, we support the notion, as already has been shown in previous studies, that

<sup>&</sup>lt;sup>2</sup> Tata Institute of Fundamental Research, Mumbai 400 005, India

<sup>&</sup>lt;sup>3</sup>Institute of Astronomy, National Central University, Chung-Li 32054, Taiwan

polarimetry, in combination with (U - B)/(B - V) colour-colour diagram, is a useful tool for identifying non-members in a cluster.

**Key words:** polarization - dust, extinction - open clusters and associations: individual: (NGC 2281, NGC 1664, NGC 1960, Stock 8 and NGC 1893).

#### 1 INTRODUCTION

Dust properties govern several physical and chemical phenomena in the interstellar medium (ISM) and act as a tracer of local environmental conditions. When starlight passes through various components of interstellar dust grains, which are aligned to the Galactic magnetic field, the radiation becomes partially plane-polarized, typically at the level of a few percent. The nature of this polarization reveals important information regarding the shape, size and composition of interstellar dust. The detailed process(es) by which grains get aligned with the magnetic fields has (have) long been, and is still actively under study (Davis & Greenstein 1951; Dolginov 1990; Cho & Lazarian 2005). In general the dust grains tend to align with their long axis perpendicular to the magnetic field (Purcell 1979). The clue to the interstellar origin of the polarization came from the observed correlation between the degree of polarization (P) and the colour excess, E(B-V). The values of P (in visual wavelengths) for the stars with large E(B-V) are found to be in the range between zero and a maximum value given by  $P_{max}/E(B-V)=~9\%~mag^{-1}$  (Aannestad & Purcell 1973). The relation between  $P_{max}$  and the colour excess, and the variation of P with wavelength, are interpreted in terms of the grain properties and the efficiency of the grain alignment. Therefore, polarimetry is a useful technique to investigate the properties like maximum polarization  $P_{\lambda_{max}}$ , the wavelength  $\lambda_{max}$  corresponding to  $P_{\lambda_{max}}$  and the orientation of the magnetic field in various Galactic locations.

The photometric and spectroscopic information already available for stars in open clusters are specifically important to make a meaningful study of the dust grains located in the foreground and in the intracluster regions (e.g., Trumpler 27, Feinstein et al. 2000; NGC 6231, Feinstein et al. 2003; Stock 16, Feinstein et al. 2003; Hogg 22 & NGC 6204, Martínez et al. 2004; NGC 5606, Orsatti et al. 2007; NGC 5749, Vergne et al. 2007; IC 1805, Medhi et al. 2007; NGC 6250, Feinstein et al. 2008; NGC 654, Medhi et al. 2008; NGC 6124, Vergne

Table 1. The basic parameters of the clusters.

Cluster Id	l (°)	b (°)	Distance (pc)	$E(B-V) \\ (mag)$	$\log(\text{age})$ $(yr)$	Reference
NGC 2281	174.90	+16.88	558	0.06, 0.11	8.70	Karchenko et al. (2005), Glaspey (1987)
NGC 1664	161.68	-0.45	1199	0.25	8.72	Karchenko et al. (2005)
NGC 1960	174.54	+1.07	1330	0.22	7.40	Sharma et al. (2006)
Stock 8	173.37	-0.18	2050	0.40 - 0.60	6.00 - 6.70	Jose et al. (2008)
NGC 1893	173.59	-1.68	3250	0.40 - 0.60	6.60	Sharma et al. (2007)

Table 2. The observational details

Cluster Id	Date of Observation (year, month, date)	Passband(s)
NGC 2281	2009, 12, 24	V
NGC 1664	2009, 12, 24	V
NGC 1960	2009, 11, 23	V
Stock 8	2009, 11, 23	V
NGC 1893	2008,11,8&9	$BV(RI)_c$

et al. 2010; NGC 6823, Medhi et al. 2010). In this paper, we present multi-wavelength polarimetry of stars towards NGC 1893. We also present V-band polarimetry of stars towards four additional clusters, viz NGC 2281, NGC 1664, NGC 1960 and Stock 8, to get information about the ISM foreground to the cluster NGC 1893. The main aim of this study is to investigate the dust properties as a function of distance towards the anticenter direction of the Galaxy ( $l \sim 160^{\circ}$  to 175°) using stars in open clusters.

The basic parameters of the observed clusters are given in Table 1. Using these five open clusters, we have made an attempt to study the dust properties of the ISM distributed between  $\sim 600$  pc (NGC 2281) and  $\sim 3$  kpc (NGC 1893). The paper is organized in the following manner. In section 2, we present a brief discussion on the observations and data reduction. We present our results in section 3, and analysis and discussion in section 4. The dust components responsible for the observed polarization are discussed in section 5. We conclude our results in section 6.

#### 2 OBSERVATIONS AND DATA REDUCTION

Polarimetric observations were carried out using the ARIES Imaging Polarimeter (AIMPOL: Rautela, Joshi & Pandey, 2004; Medhi et al. 2007, 2010) mounted at the Cassegrain focus of the 104-cm Sampurnanand telescope of the Aryabhatta Research Institute of observational sciencES (ARIES), Nainital, India, coupled with a TK 1024×1024 pixel<sup>2</sup> CCD camera. The AIMPOL consists of a half-wave plate (HWP) modulator and a Wollaston prism beam-

splitter. The observations were carried out in B, V,  $R_c$  and  $I_c$  ( $\lambda_{B_{eff}}$ =0.440  $\mu$ m,  $\lambda_{V_{eff}}$ =0.530  $\mu$ m,  $\lambda_{Rc_{eff}}$ =0.670  $\mu$ m and  $\lambda_{I_{eff}}$ =0.800  $\mu$ m) photometric bands. Details of the observations are given in Table 2. Each pixel of the CCD corresponds to 1.73 arcsec and the field-of-view is  $\sim 8$  arcmin in diameter. The FWHM of the stellar image varied from 2 to 3 pixels. The read out noise and gain of the CCD are 7.0  $e^{-1}$  and 11.98  $e^{-1}$ /ADU, respectively. Due to the absence of a grid in AIMPOL, we manually checked for any overlap of ordinary and extra-ordinary images of the sources.

Fluxes of ordinary  $(I_o)$  and extra-ordinary  $(I_e)$  beams for all the observed sources with good signal-to-noise ratio were extracted by standard aperture photometry after bias subtraction using the IRAF<sup>1</sup> package. The ratio  $R(\alpha)$  is given by:

$$R(\alpha) = \frac{\frac{I_e(\alpha)}{I_o(\alpha)} - 1}{\frac{I_e(\alpha)}{I_o(\alpha)} + 1} = P\cos(2\theta - 4\alpha),\tag{1}$$

where P is the fraction of the total linearly polarized light and  $\theta$  is the polarization angle of the plane of polarization. Here  $\alpha$  is the position of the fast axis of the HWP at 0°, 22.5°, 45° and 67.5° corresponding to the four normalized Stokes parameters respectively, q [R(0°)], u [R(22.5°)],  $q_1$  [R(45°)] and  $u_1$  [R(67.5°)]. The detailed procedures used to estimate the polarization and polarization angles for the programme stars are described by Ramaprakash et al. (1998), Rautela, Pandey, & Joshi (2004) and Medhi et al. (2010). Since polarization accuracy is, in principle, limited by photon statistics, we estimated the errors in normalized Stokes parameters  $\sigma_{R(\alpha)}$  ( $\sigma_q$ ,  $\sigma_u$ ,  $\sigma_{q_1}$  and  $\sigma_{u_1}$  in %) using the expression (Ramaprakash et al. 1998):

$$\sigma_{R(\alpha)} = \sqrt{(N_e + N_o + 2N_b)/(N_e + N_o)} \tag{2}$$

where  $N_e$  and  $N_o$  are the counts in extra-ordinary and ordinary rays respectively, and  $N_b[=\frac{N_{be}+N_{bo}}{2}]$  is the average background counts around the extra-ordinary and ordinary rays of a source. The individual errors associated with the four values of  $R(\alpha)$ , estimated using equation (2), are used as weights in calculation of P and  $\theta$  for the programme stars.

To correct the measurements for null polarization (or instrumental polarization) and the zero-point polarization angle, we observed several polarized and unpolarized standards taken from Schmidt, Elston & Lupie (1992). The results on polarized and unpolarized standards are given in Table 3. The values of  $\theta$  are in equatorial coordinate system measured from the North increasing towards the East. Both the observed degree of polarization [P(%)]

<sup>&</sup>lt;sup>1</sup> IRAF is distributed by National Optical Astronomical Observatories, USA.

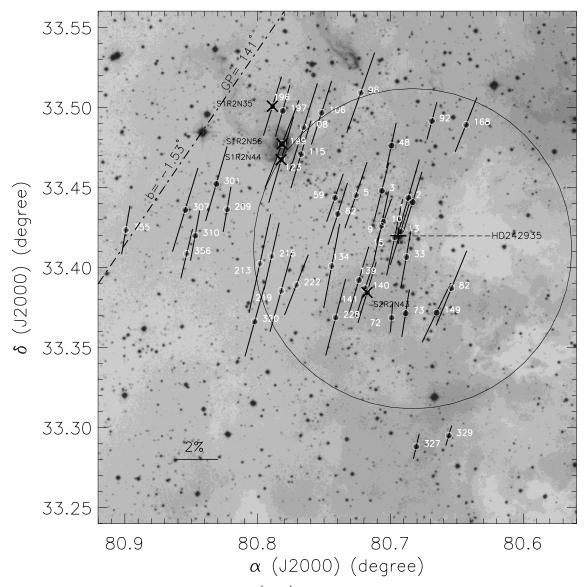


Figure 1. Stellar polarization superimposed on the  $20' \times 20'$  R-band DSS II image of the field containing NGC 1893. The length of each polarization vector is proportional to  $P_V$ . A vector with a polarization of 2% is drawn for reference. The dash-dotted line marks the Galactic parallel b=-1.53°. H $\alpha$  emission stars identified by Marco and Negueruela (2002) (S2R2N43) and by Negueruela et al (2007) (S1R2N35, S1R2N56 and S1R2N44) are shown with cross symbols. The identification numbers are taken from Cuffey and Shapley (1937). The circle represents the boundary ( $\sim$  6' radius, Sharma et al. 2007) of the cluster.

and polarization angle  $[\theta(°)]$  for the polarized standards are in good agreement with those given by Schmidt et al. 1992. The observed normalized Stokes parameters q and u (q%, u%) for standard unpolarized stars are also given in Table 3. The instrumental polarization of AIMPOL on the 104-cm Sampurnanand Telescope has been monitored since 2004 in different projects and found to be less than 0.1% in different bands (Rautela, Pandey, & Joshi, 2004; Medhi et al. 2007, 2008, 2010; Pandey et al. 2009).

#### 3 RESULTS

#### 3.1 NGC 1893

The polarization measurements for stars in the region of NGC 1893 are listed in Table 4. The star identification numbers (column 1) are taken from Cuffey and Shapley (1937). The V-band magnitudes are given in column 2. The degree of polarization P (in percent) and polarization angles  $\theta$  (in degree) measured in B, V,  $(R, I)_c$  bands and their corresponding standard errors ( $\epsilon_P$  and  $\epsilon_\theta$ ) are given in columns 3 to 10.

The sky projection of the V-band polarization vectors for the 44 stars measured towards the NGC 1893 region is drawn on the R-band Digitized Sky Survey II (DSS II) image (Fig. 1). The length of each polarization vector is proportional to the degree of polarization. A vector with a polarization of 2% is drawn for reference. The dash-dotted line superimposed in Fig. 1 is indicating the orientation of the projection of the Galactic plane (GP) which has a polarization angle of  $\theta_{GP} = 141^{\circ}$ . The average polarization (P) and polarization angle ( $\theta$ ) for 44 stars are found to be  $2.4 \pm 0.6\%$ ,  $160 \pm 5^{\circ}$  in B,  $2.6 \pm 0.7\%$ ,  $162 \pm 5^{\circ}$  in V,  $2.5 \pm 0.7\%$ ,  $159 \pm 6^{\circ}$  in  $R_c$  and  $2.2 \pm 0.5\%$ ,  $161 \pm 6^{\circ}$  in  $I_c$  bands, respectively.

#### 3.2 NGC 2281, NGC 1664, NGC 1960 and Stock 8

Polarimetric measurements in V-band for 14 stars towards NGC 2281, 27 stars towards NGC 1664, 15 stars towards NGC 1960 and 21 stars towards Stock 8, have also been carried out. The results are listed in Tables 5, 6, 7 and 8 respectively. The star identification numbers for NGC 2281, NGC 1664, NGC 1960 and Stock 8 are taken from Vasileviskis & Balz (1959), Larsson-Leander (1957), Boden (1951) and Mayer (1964) respectively.

The mean values of  $P_V$  and  $\theta_V$  towards NGC 2281, NGC 1664, NGC 1960 and Stock 8 are found to be  $0.9 \pm 0.2\%$  and  $16 \pm 6^\circ$ ;  $1.8 \pm 0.7\%$  and  $172 \pm 8^\circ$ ;  $1.2 \pm 0.2\%$  and  $159 \pm 5^\circ$  and  $2.4 \pm 0.6\%$  &  $160 \pm 7^\circ$ , respectively.

#### 4 ANALYSIS AND DISCUSSION

Fig. 2 presents the distribution of  $P_V$  and  $\theta_V$  for stars in the observed cluster regions. Four clusters studied here, namely NGC 1664, NGC 1960, Stock 8 and NGC 1893 are located at Galactic latitude  $|b| < 2^{\circ}$ . The nearest open cluster NGC 2281 studied here is located at  $b = +16.88^{\circ}$ . A Gaussian fit to the distribution of  $P_V$  and  $\theta_V$  yields a mean and a standard

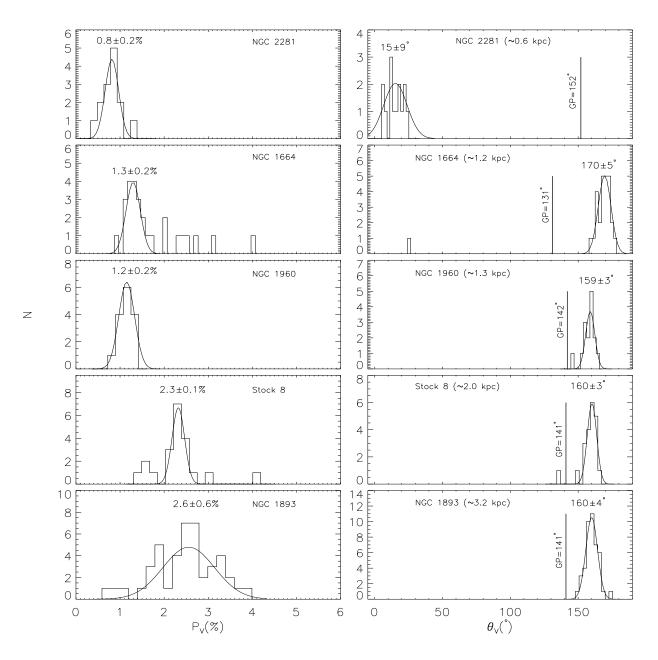


Figure 2. Histograms for  $P_V$  (left panel) and  $\theta_V$  (right panel) in five observed clusters, NGC 2281, NGC 1664, NGC 1960, Stock 8 and NGC 1893. The polarization angle for the Galactic plane of each cluster is shown with a continuous line and is labeled with GP. Each histogram is fitted with a Gaussian function.

deviation as  $0.8 \pm 0.2\%$  and  $15 \pm 9^\circ$  for NGC 2281;  $1.3 \pm 0.2\%$  and  $170 \pm 5^\circ$  for NGC 1664;  $1.2 \pm 0.2\%$  and  $159 \pm 3^\circ$  for NGC 1960;  $2.3 \pm 0.1\%$  and  $160 \pm 3^\circ$  for Stock 8; and  $2.6 \pm 0.6\%$  and  $160 \pm 4^\circ$  for NGC 1893. It is evident from Fig. 2 that the mean value of  $P_V$  increase with the distance of a cluster.

The polarization angle corresponding to the Galactic plane for each cluster is drawn with a continuous line. Fig. 2 (right panel) indicates that the difference between GP and mean  $\theta_V$  is the largest for the nearby least polarized (0.8 ± 0.2%) cluster (NGC 2281:  $l=174.90^{\circ}$ 

and  $b=+16.88^{\circ}$ ). Whereas, in the case of four clusters, namely NGC 1664, NGC 1960, Stock 8 and NGC 1893, the difference between GP and mean  $\theta_V$  (Gaussian) is small and is almost the same. Fig. 2 also reveals that in the Galactic longitude range  $l \sim 160^{\circ}$  to  $\sim 175^{\circ}$  and within the Galactic plane ( $|b| < 2^{\circ}$ ), the polarization angles remain almost constant. The average of the mean values of polarization angles for the four clusters is found to be 163° with a standard deviation of 6°. This implies that at least beyond  $\sim 1$  kpc the magnetic field orientation remains almost unchanged. However, for a smaller distance ( $\sim 0.6$  kpc), the polarization angle towards the northern hemisphere (NGC 2281) of the Galactic plane is found to be 16° with a standard deviation of 6°.

The polarization towards the Taurus molecular complex ( $l = 174.13^{\circ}$ ,  $b = -13.45^{\circ}$ ), taken from Heiles (2000), reveals a mean polarization angle of 58° with a standard deviation of 38°. The region selected around the Taurus molecular complex is bound between the Galactic longitude  $l = 160^{\circ}$  to 175° and latitude  $b < -2^{\circ}$ . It is interesting to mention that, the mean polarization angles at high Galactic latitude ( $|b| > 2^{\circ}$ ) are significantly different from those in the Galactic plane  $|b| < 2^{\circ}$ .

#### 4.1 Member identification

The individual Stokes parameters of the polarization vector of the V-band,  $P_V$ , given by  $Q_V = P_V \cos(2\theta_V)$  and  $U_V = P_V \sin(2\theta_V)$  are estimated for all the observed stars towards five clusters and presented on a  $U_V$  versus  $Q_V$  plot in Fig. 3. In such a diagram, members of a star cluster are expected to group together, while non-members are expected to show a scattered distribution. The reason is that the measured polarization of a star depends on the column density of aligned dust grains that lie in front of the star and hence the degree of polarization would be similar, lower or higher depending on whether the star is a cluster member, a foreground or a background to the cluster. Likewise, the polarization angles of cluster members would be similar but could be different for foreground or background non-member stars as light from them could have contributions from different or additional dust components. Therefore  $U_V - Q_V$  plot could be a useful tool to segregate the members and non-members of a cluster. Stars with intrinsic polarization, e.g., due to an asymmetric distribution of matter around young stellar objects (YSOs) and/or rotation in their polarization angles (see section 4.2) may also create scattered distribution in the  $U_V - Q_V$  plane.

As shown in Fig. 3, in the case of nearby clusters viz NGC 2281, NGC 1664 and NGC

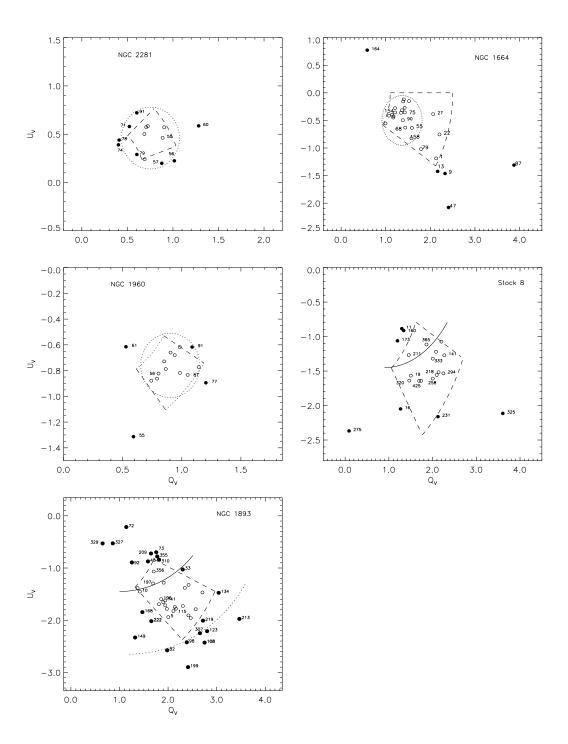


Figure 3. The  $U_V$  versus  $Q_V$  diagrams for stars towards NGC 2281, NGC 1664, NGC 1960, Stock 8 and NGC 1893 cluster regions, measured in the V-band. In each case a box with dashed line marks the boundary of mean  $P_V \pm \sigma$  and mean  $\theta_V \pm \sigma$ . Stars lying outside the  $1\sigma$  box are shown by filled circles. It can be seen that the majority of the stars of apparent grouping lie within the box (open circles). The apparent grouping in the case of NGC 2281, NGC 1664 and NGC 1960 is bound by a dotted circle. The thin continuous curve in the case of Stock 8 and NGC 1893 separates foreground field stars from cluster members. The dotted curve in the case of NGC 1893 demarcates the stars having relatively high polarization and high E(B-V) values as well as having intrinsic polarization (see the text).

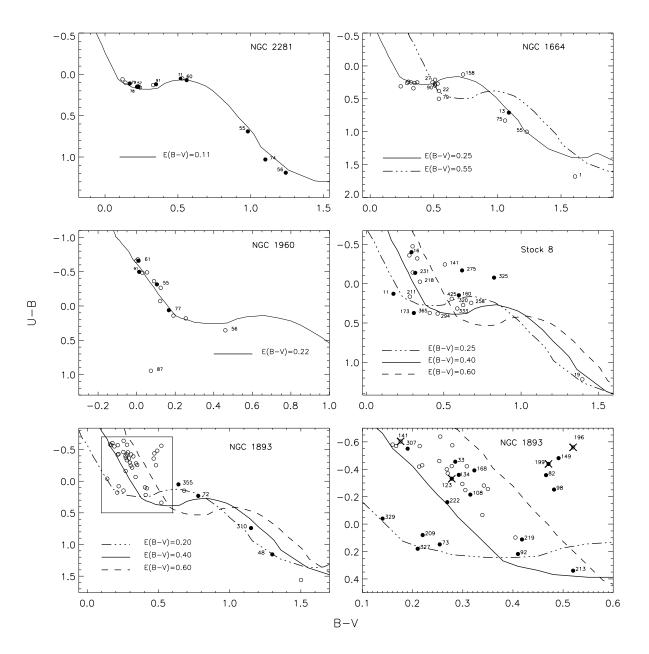


Figure 4. (U-B) versus (B-V) colour-colour diagram for the stars in the cluster region. Theoretical zero-age-main sequence (ZAMS) is taken from Schmidt-Kaler (1982) and is shifted along a reddening vector with an adopted slope of E(U-B)/E(B-V)=0.72, to match the observed colours. The symbols are same as in Fig. 3. In the case of NGC 1893, the H $\alpha$  emission stars are indicated with cross symbols. The lowermost-right panel shows the enlarged view of the colour-colour diagram shown within the inset of NGC 1893 colour-colour diagram (lower left panel).

1960, a grouping (bound visually by the dotted circle) is apparent, whereas in the case of distant clusters i.e. Stock 8 and NGC 1893, the  $U_V - Q_V$  diagram shows a scattered distribution. A scattered distribution in the case of a distant cluster is expected as the cluster region is contaminated by foreground/ background field stars. Moreover, clusters Stock 8 and NGC 1893 are young and have differential reddening, hence cluster matter may

also affect the polarization. The apparent clustering in the case of NGC 2281, NGC 1664 and NGC 1960 further supports the above notion as these are relatively nearby clusters and have less field star contamination. Since these clusters are of intermediate age ( $\gtrsim 25$  Myr), the effect of variable reddening is absent. The distribution is significantly scattered in the case of NGC 1893, which is the most distant cluster in the present study. It seems difficult to identify probable cluster members of NGC 1893 using the  $U_V - Q_V$  diagram as shown in Fig. 3. To further elucidate the membership in the clusters which do not show any apparent grouping we plot a box with dashed line in  $U_V - Q_V$  plots (Fig. 3) having boundaries of mean  $P_V \pm \sigma$  and mean  $\theta_V \pm \sigma$  (as mentioned in section 3). It can be seen that the majority of stars of apparent grouping lie within the boundaries of the box as mentioned above. Therefore, in the case of clusters, where grouping is absent (Stock 8 and NGC 1893), we presume that the stars lying within the  $1\sigma$  box of mean  $P_V$  and  $\theta_V$  values are probable members of the cluster.

The combination of  $U_V - Q_V$  diagram and (U - B)/(B - V) colour-colour diagram can yield a better identification of probable members in a distant cluster (see e.g. Haikala 1995, Feinstein et al. 2008). Fig. 4 shows the (U - B)/(B - V) colour-colour diagram for NGC 2281, NGC 1664, NGC 1960, Stock 8 and NGC 1893 cluster regions. For the clusters NGC 2281, NGC 1664, NGC 1960 and Stock 8, the (B - V) and (U - B) colours are taken from the Tables 5, 6, 7 and 8 respectively, whereas for the cluster NGC 1893, the colours are taken from Sharma et al. (2007) and Massey et al. (1995). The continuous curve represents the reddened ZAMS for the cluster region as per E(B - V) values mentioned in Table 1. In Fig. 3, the stars lying within the  $1\sigma$  box are shown by open circles, whereas stars outside the  $1\sigma$  box are shown by filled circles. It is apparent from Fig. 3 that stars located within the  $1\sigma$  box follow the general reddening of the cluster region, hence may be probable members of the clusters. On the basis of Figs 3 and 4, we can draw the following conclusions:

NGC 2281: All the stars lying within the  $1\sigma$  box and the boundary of apparent grouping follow the ZAMS reddened for E(B-V) (=0.11 mag) of the cluster region. Although stars #55, 56 and 74 lie on the reddened ZAMS, they have  $(B-V) \gtrsim 1.0$ . These stars could not be MS members of the cluster having  $\log(\text{age}) = 8.7$  yr. The star #60 is located away from the grouping (Fig. 3). However it follows the reddened ZAMS and its colours are comparable to the probable MS members.

NGC 1664: Stars located within the region bound by a dotted circle (see Fig. 3) have  $P_V \lesssim 2\%$  and nicely follow the ZAMS reddened by E(B-V) = 0.25 mag. Hence these could be

probable members of the cluster. The stars #1, 22, 27 and 79 are located outside the circle but within the  $1\sigma$  box. These stars show polarization in the range  $2.0 \lesssim P_V \lesssim 2.5\%$  and follow the ZAMS reddened by  $E(B-V) \sim 0.55$  mag. Stars #9, 13, 47 and 87 lie outside the  $1\sigma$  box. These stars show  $P_V$  values ranging from 2.5-4.1 %. These two groups of stars should be background stars. Star #13 has  $P_V=2.59\%$ , but its estimated  $E(B-V) \sim 0.25$  is comparable to the cluster's E(B-V) value. As the age of the cluster is  $\sim 500$  Myr, the star #13 (V=14.36, B-V=1.09) could not be a MS member. Star #164, located significantly away from the grouping, is the lowest polarized star (0.97%) and its polarization angle is significantly different ( $26\pm7^{\circ}$ ) from those of the remaining stars of the region. It should be a foreground non-member.

NGC 1960: The stars located within the bound region and the  $1\sigma$  box indicate  $E(B-V) \sim 0.22$  mag. Star #55 is located significantly away from the general distribution, but follows the ZAMS reddened by the average reddening of the region (cf. Fig. 4). This star has relatively a high polarization ( $P_V = 1.44 \pm 0.24\%$ ) and small polarization angle ( $\theta_V = 147 \pm 5^\circ$ ) in comparison to the remaining stars of the region. It should be a background field star. Star #61, the least polarized star ( $P_V = 0.81\%$ ) of the region, lies on the reddened ZAMS, but is located away from the general distribution. We conclude that star #61 is probably a foreground field star. Although star #77 is located beyond the  $1\sigma$  box, it follows the reddened ZAMS. This star has polarization  $P_V = 1.50 \pm 0.31\%$  and could be a background non-member. Star #91 seems to be associated with the apparent grouping. Its polarization ( $P_V = 1.25 \pm 0.14\%$ ) is comparable to the cluster mean  $P_V$  value, hence it could be a member of the cluster.

Stock 8: The  $U_V - Q_V$  diagram does not show any grouping. The (U - B)/(B - V) colour-colour diagram indicates that barring stars #211 and 365, the remaining stars lying within the  $1\sigma$  box have E(B - V) in the range of 0.40 - 0.60 mag, hence should be members of the cluster. Stars #11, 160 and 173 lie outside the  $1\sigma$  box. These three stars, along with stars #19, 211 and 365, have  $E(B - V) \sim 0.25$  mag. Hence these should be foreground stars. Stars #16 and 231 are distributed near the edge of the  $1\sigma$  box and have E(B - V) and polarization values comparable to the mean values for the cluster region. These two stars could be cluster members. The stars #275 and 325 are located out side the  $1\sigma$  box, however they seem to be reddened B type stars of the region (cf. Fig. 4). Star #275 has significantly different polarization angle  $(136\pm 5^{\circ})$  from the mean value for the cluster region  $(160\pm 7^{\circ})$ , although the polarization value  $(2.37\pm 0.39\%)$  is similar to the cluster mean value

 $(2.40\pm0.60\%)$ . Star #325 has a relatively higher  $P_V$   $(4.18\pm0.44\%)$  value than the mean value for the cluster region  $(2.40\pm0.60\%)$  although the polarization angle  $(165\pm3^{\circ})$  is similar to the cluster mean value  $(160\pm7^{\circ})$ . Hence the membership determination of these two stars, #275 and 325, is uncertain. The approximate boundary to demarcate the foreground stars from the cluster members is shown by a thin continuous curve (see Fig. 3).

NGC 1893: The colour-colour diagram of the region reveals that barring stars #197 and 356, all the stars lying within the  $1\sigma$  box have  $E(B-V)\sim 0.4-0.6$  mag, indicating that these stars may be cluster members. Fig. 4 reveals that stars #48, 72, 73, 92, 209, 310, 327, 329 and 355 have  $E(B-V) \sim 0.2$  mag, hence these should be field stars. Five stars #33, 134, 168, 219 and 222 are located near the boundary of the  $1\sigma$  box. These stars have E(B-V) in the range of 0.40–0.60 mag, hence these could also be members of the cluster. Star #149 is apparently located away from the distribution. This star has relatively higher value of  $\overline{\epsilon}$  (2.43; cf. Sec. 4.2 and Table 9) and may have a rotation in the polarization angle. Two stars #141 (S2R2N43, Marco and Negueruela 2002) and #196 (S1R2N35, Negueruela et al. 2007) are  $H\alpha$  emission stars. On the basis of polarization, reddening and position in the  $U_V - Q_V$  plot, star #141 should be a cluster member. However, star #196 is a highly reddened MS star (E(B-V)=0.83) and is probably an HAe/Be star (see Fig. 8), but its  $P_V$  (2.45 ± 0.29%) and  $\theta_V$  (160 ± 3°) suggest that it could have undergone depolarization effect. Hence, the membership of star #196 is uncertain. The stars having relatively high polarization and high E(B-V) values as well as having intrinsic component of polarization have been demarcated using a dotted curve as shown in Fig. 3. Fig. 4 indicates that stars #82 and 98 are highly reddened stars, whereas 123 and 199 are  $H\alpha$  emission stars with possible intrinsic component of polarization. Star #108 seems to be a classical Be star (cf. Fig. 8) and may have an intrinsic component of polarization. Star #213 may have rotation in its polarization angle as its  $\overline{\epsilon} = 1.45$  (see Table 9).

The probable members of the cluster identified using  $U_V - Q_V$  and colour-colour diagrams, along with the kinematic membership probability  $(M_P)$  taken from Vasileviskis & Balz (1959) for NGC 2281 and from Dias et al. (2006) for remaining clusters, are mentioned in Tables 5, 6, 7, 8 and 9. Stars with kinematic membership probability  $\geq 50\%$  are considered as members. The member and non-member stars are represented with M and NM respectively. Stars with uncertainty in their membership determination are indicated with a '?' symbol. A comparison indicates that the discrepancy between the membership estimated

from kinematic criterion and in the present work is  $\sim 15\%-20\%$  for the nearby clusters (i.e., NGC 2281, NGC 1664 and NGC 1960). The discrepancy is found to increase ( $\sim 30\%-45\%$ ) for distant clusters (i.e., Stock 8 and NGC 1893). The mean values of  $P_V$  and  $\theta_V$  of member stars of the respective clusters as identified above as well as of field stars lying in the cluster regions are given in Table 10. The mean values of  $P_V$  for members of the two nearby clusters viz NGC 2281 and NGC 1960 are the same as those for field stars in these regions, whereas in the case of other nearby cluster (NGC 1664), the non-members show higher value for mean  $P_V$ . The higher values of  $P_V$  for field stars towards the direction of cluster NGC 1664 are due to the fact that the non-member field stars are located in the background of the cluster and have higher extinction (see Fig. 4). In the case of the distant clusters Stock 8 and NGC 1893, the mean values of  $P_V$  for non-members are lower than those for member stars. The mean values of  $P_V$  obtained for cluster members further manifest an increasing trend with distance. Table 10 also indicates that the mean  $\theta_V$  values are almost the same for members and non-members lying towards the direction of the clusters studied in the present work.

The  $U_V - Q_V$  plot is also a useful tool to study the interstellar dust distribution as a function of distance from the Sun to the clusters (e.g., Feinstein et al. 2008). The clusters studied in the present work have distances in the range of  $\sim 0.6$  to  $\sim 3$  kpc. The polarimetric results obtained can be used to study the properties of the dust towards the anticenter direction ( $l\sim 160^\circ$  -  $175^\circ$ ) of the Galaxy. Based upon the earlier discussion using  $Q_V-U_V$ and (U-B)/(B-V) diagrams, in Fig. 5 we show a combined  $U_V-Q_V$  diagram for all the five clusters, namely, NGC 2281 (inverted triangles), NGC 1664 (squares), NGC 1960 (triangles), Stock 8 (circles) and NGC 1893 (star symbols). Open and filled symbols are used to represent members and non-members based upon our analysis. The dust free environment of the solar neighbourhood (shown with rectangular box) is represented by  $Q_V = 0$  and  $U_V = 0$ , while any other point on this plot represents the direction of the polarization vector seen towards that direction from the Sun. Fig. 5 suggests that the degree of polarization of stars is found to increase with the distance to the clusters, as also noticed in Fig. 2. This is consistent with the fact that the degree of polarization increases with the column density of dust grains lying in front of the stars that are relatively well aligned. The close proximity of the points of NGC 1664 and NGC 1960 in  $U_V - Q_V$  plane is consistent with the fact that they are located approximately at similar distances (1.2 and 1.3 kpc, respectively).

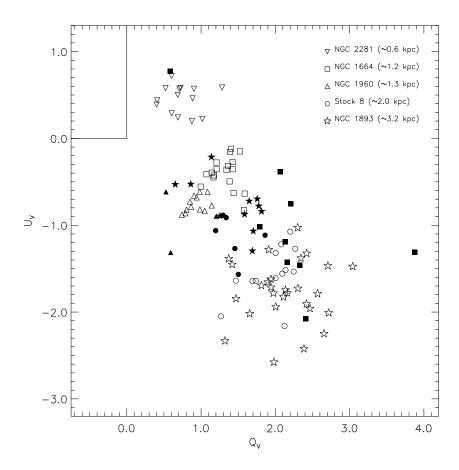


Figure 5. The  $U_V$  versus  $Q_V$  diagram for stars lying in the cluster regions studied, namely, NGC 2281 (inverted triangles), NGC 1664 (squares), NGC 1660 (triangles), Stock 8 (circles) and NGC 1893 (star symbols). The filled symbols represent field stars in the respective cluster regions. The rectangular box covered by  $Q_V = 0$  and  $U_V = 0$  is the dust free environment of the solar neighbourhood.

#### 4.2 The Serkowski law

The wavelength dependence of polarization towards many Galactic directions follows the Serkowski's law of interstellar polarization (Serkowski 1973; Coyne, Gehrels & Serkowski 1974; Wilking, Lebofsky, & Rieke 1982):

$$P_{\lambda} = P_{max} \exp[-K \ln^2(\lambda_{max}/\lambda)] \tag{3}$$

Where  $P_{\lambda}$  is the percentage polarization at wavelength  $\lambda$  and  $P_{max}$  is the peak polarization, occurring at wavelength  $\lambda_{max}$ . The  $\lambda_{max}$  is a function of optical properties and characteristic particle size distribution of aligned grains (Serkowski, Mathewson & Ford, 1975; McMillan, 1978). The value of  $P_{max}$  is determined by the column density, the chemical composition, size, shape, and alignment efficiency of the dust grains. The parameter K, an inverse measure of the width of the polarization curve, was treated as a constant by Serkowski et al. (1975), who adopted a value of 1.15 for all the stars. The Serkowski's relation with K=1.15 provides an

adequate representation of the observations of interstellar polarization between wavelengths 0.36 and  $1.0 \mu m$ . If the polarization is produced by aligned interstellar dust grains, the observed data will follow equation (3) and hence we can estimate  $P_{max}$  and  $\lambda_{max}$  for each star. The  $P_{max}$  and  $\lambda_{max}$  are obtained using the weighted least-squares fitting to the measured polarization in  $BV(RI)_c$  bands to equation (3) by adopting K=1.15. We have also computed the parameter  $\sigma_1^2$  (the unit weight error of the fit) for each star that quantifies the departure of the data points from the standard Serkowski's law. Because of the weighting scheme, the values of  $\sigma_1$  should not exceed 1.5, but if they do, it implies that the stars have intrinsic polarization (e.g., Feinstein et al. 2008, Medhi et al 2007, 2008, 2010). The  $\lambda_{max}$  values can also be used to infer the origin of the polarization. The stars with  $\lambda_{max}$  much lower than the average value of the interstellar medium (0.545  $\mu$ m; Serkowski, Mathewson & Ford 1975) may have an intrinsic component of polarization. Another parameter to infer the presence of intrinsic polarization or polarization angle rotation along the line of sight (Coyne 1974, Martin 1974), is the dispersion of the polarization angle for each star normalized by the average of the polarization angle errors,  $\bar{\epsilon}$  (Marraco et al. 1993; Orsatti et al. 2007; Feinstein et al. 2008).

The estimated values of  $P_{max}$ ,  $\lambda_{max}$ ,  $\sigma_1$  and  $\overline{\epsilon}$  for the stars towards NGC 1893 are given in Table 9. The star identifications are same as given in Table 4. The weighted mean values of the  $P_{max}$  and  $\lambda_{max}$  are found to be  $2.59 \pm 0.02\%$  and  $0.55 \pm 0.01~\mu m$  respectively. The estimated  $\lambda_{max}$  is quite similar to the value corresponding to the general interstellar medium  $(0.545~\mu m)$ , Serkowski et al. 1975). Using the relation  $R_V = 5.6 \times \lambda_{max}$  (Whittet & Van Breda 1978), the value of  $R_V$ , the total-to-selective extinction, comes out to be  $3.08 \pm 0.05$ , which is in agreement with the average value  $(R_V = 3.1)$  for the Milky Way Galaxy, indicating that the size of the dust grains within the cluster NGC 1893 is normal. Similar conclusion was drawn by Sharma et al. (2007) using  $(\lambda - V)/(B - V)$  two colour diagrams. In Fig. 6 we show  $\sigma_1$  versus  $P_{max}$  (upper panel) and  $\overline{\epsilon}$  versus  $\lambda_{max}$  (lower panel) plots. The criteria mentioned above indicate that majority of the stars do not show evidence of intrinsic polarization. However a few stars #72, 149, 199, 209 and 215 show deviation from the general distribution.

Star #199 is an  $H\alpha$  emission star and its location in the V/(V-I) colour-magnitude diagram (CMD) (Fig. 7) reveals that it should be a pre-main sequence (PMS) star. The

<sup>&</sup>lt;sup>2</sup> The values of  $\sigma_1$  for each star are computed using the expression  $\sigma_1^2 = \sum (r_{\lambda}/\epsilon_{p\lambda})^2/(m-2)$ ; where m is the number of colours and  $r_{\lambda} = P_{\lambda} - P_{max} \exp[-K \ln^2(\lambda_{max}/\lambda)]$ .

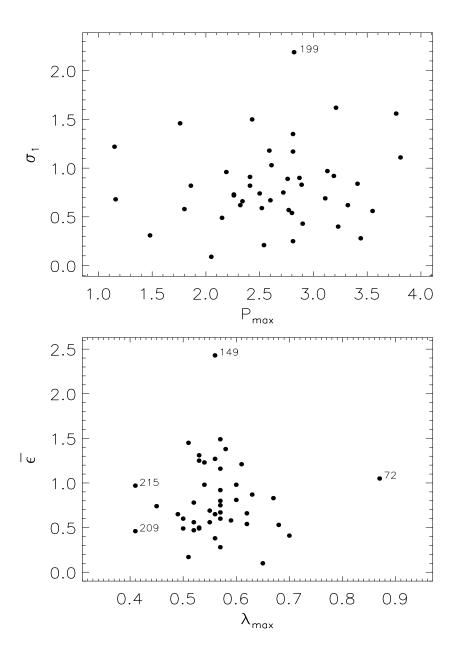


Figure 6. Top panel is the plot between  $\sigma_1$  and  $P_{max}$ , whereas the bottom panel is the plot between  $\bar{\epsilon}$  versus  $\lambda_{max}$ .

location of star #209 in the (U-B)/(B-V) colour-colour diagram (Fig. 4) suggests that it could be a foreground field star. The V/(V-I) CMD reveals that star #215 should be a PMS star. Star #123 and 199 are identified as  $H\alpha$  emission stars S1R2N44 and S1R2N56, respectively (Neguerela et al. 2007). Stars #199 and 215 are likely to be PMS stars and accreting matter from their circumstellar material. The accreted material, probably distributed in an asymmetric disk geometry, might be responsible for the observed intrinsic component

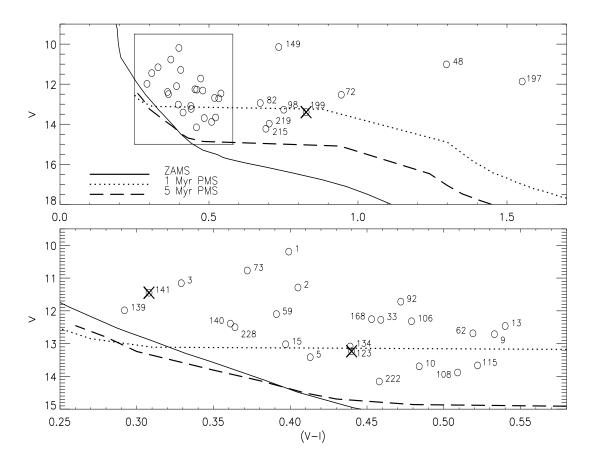


Figure 7. Upper panel is the V versus (V-I) colour-magnitude diagram for the NGC 1893 region. The continuous, dotted and dashed curves represent the ZAMS from Girardi et al. (2002) and PMS isochrones for 1 and 5 Myr by Siess et al. (2000) respectively. The isochrones are adjusted for a distance of 3.2 kpc and E(B-V)=0.40 mag. The stars having  $H\alpha$  emission are shown by crosses. The lower panel is the enlarged view of the colour-magnitude diagram shown in the inset of the upper panel.

of polarization. The computed values of  $\bar{\epsilon}$  show no significant rotation (except for star #149) in polarization angles reiterating the fact that the dust component responsible for the measured polarization is well aligned. Star #149 is a highly reddened MS star (see. Figs 4, 7 and 8) as it is embedded at the eastern edge of the wind blown bubble (cf. Sharma et al. 2007).

#### 4.3 Polarization efficiency

The degree of polarization produced for a given amount of extinction (or reddening) is referred as the polarization efficiency of the intervening dust grains. The polarization efficiency depends mainly on the orientation of the magnetic field along the line of sight, the magnetic field strength and the degree of alignment of the dust grains. Mie calculations place a theoretical upper limit of  $P_{max} = 43 \times E(B-V)$  (Whittet 1992 and references there

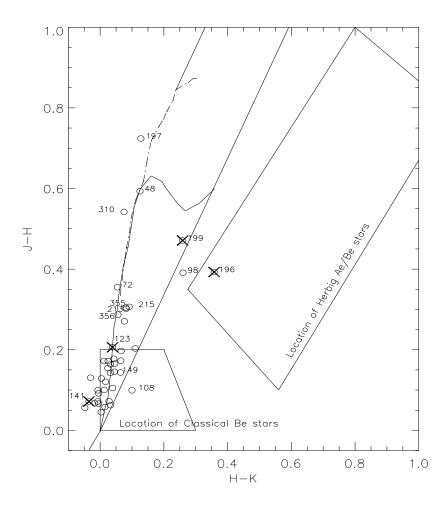


Figure 8. (J-H) versus (H-K) colour-colour diagram for the NGC 1893 region. The data is taken from the Two-Micron All-Sky Survey (2MASS) Point Source Catalog (PSC) (Cutri et al. 2003). 2MASS data has been converted in to California Institute of Technology (CIT) system using the relations provided by Carpenter (2001). The theoretical tracks for dwarfs and giants are drawn (Bessell & Brett, 1988). Reddening vectors are also drawn (Cohen et al. 1981). The location of Be stars (cf. Dougherty et al. 1994), and the location of Herbig Ae/Be stars (cf. Hernandez et al. 2005) are also shown. The stars having  $H\alpha$  emission are shown by crosses.

in) on the polarization efficiency by an infinite cylinder with the diameter comparable to the wavelength of the incident light and with their long axes parallel to each other and perpendicular to the line of sight. The empirical upper limit relation for the polarization efficiency resulting from the studies of reddened Galactic stars, assuming normal interstellar material characterized by  $R_V = 3.1$  (Serkowski, Mathewson & Ford 1975) is found to be  $P_{max} = 9 \times E(B-V)$ . The fact that the maximum observed polarization efficiency is found to be less by a factor of 4.8 than that expected from theory, implies that the alignment of dust grains is not perfect. The reason could be the presence of various components of magnetic fields oriented differently along the line of sight and/or the grains are only moderately elongated rather than infinite cylinder.

The UBV photometric data by Sharma et al. (2007) and Massey et al. (1995) have been

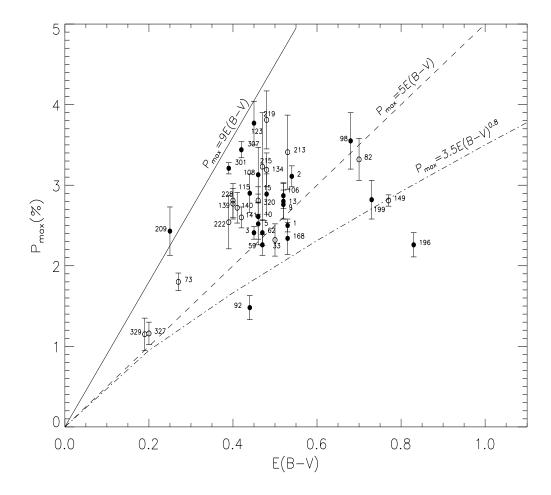


Figure 9. The polarization efficiency diagram. Filled and open circles are the stars distributed in the northern and southern regions of the cluster respectively. The solid line represents the empirical upper limit relation for the polarization efficiency of  $P_{max} = 9 \times E(B-V)$  (Serkowski et al. 1975). The dashed line represents the relation  $P_{max} = 5 \times E(B-V)$  (Serkowski et al. 1975) and the dashed-dotted line represents the relation  $P_{max} = 3.5 \times E(B-V)^{0.8}$  by Fosalba et al. (2002).

used to estimate the reddening E(B-V). The reddening of individual stars having spectral type earlier than A0, has been derived using the Q method (Johnson & Morgan 1953) and the values are given in Table 9. The (J-H)/(H-K) near infrared (NIR) colour-colour diagram (Fig. 8) reveals that stars #48, 72, 197, 310, 355 and 356 have spectral type later than A0. The (U-B)/(B-V) colour-colour diagram (Fig. 4) indicates that these stars follow ZAMS reddened by E(B-V)=0.2 mag, hence we assign reddening of E(B-V)=0.20 mag.

In Fig. 9, we present  $P_{max}$  versus E(B-V) for stars towards NGC 1893 region. The continuous line shows the empirical upper limit for the polarization efficiency given by  $P_{max} = 9 \times E(B-V)$  (Serkowski et al. 1975), assuming normal interstellar material characterized by  $R_V = 3.1$ . The recent estimate of the average efficiency by Fosalba et al. (2002), which is valid for E(B-V) < 1.0 mag, is represented by the relation  $P_{max} = 3.5 \times E(B-V)^{0.8}$ 

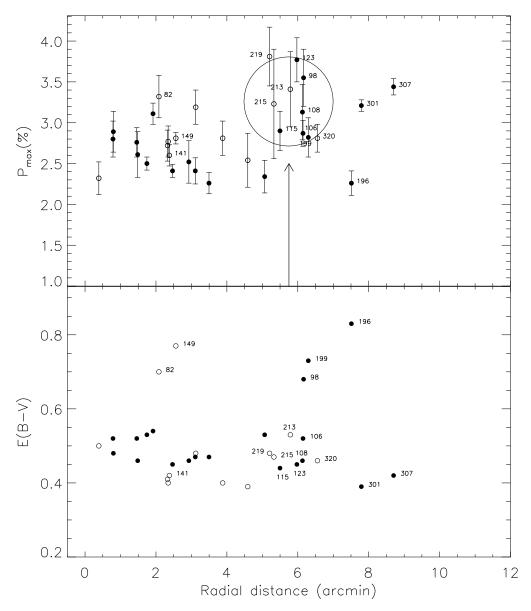


Figure 10. The radial variation of  $P_{max}$  (upper panel) and E(B-V) (lower panel) for the cluster members and the stars (# 108, 123, 196, 199 and 213) with uncertainty in their membership. Filled circles are the stars distributed in the northern part, whereas open circles are in the southern part of the cluster NGC 1893. Most of the stars falling within the circle at a distance of 5'.5 are distributed nearer the two nebulae Sim 129 and 130.

and is shown by the dash-dotted line. For comparison, the average polarization efficiency relation,  $P_{max} = 5 \times E(B - V)$  (Serkowski et al. 1975), is also drawn using the dashed line. A majority of the points are found to lie between the continuous line and above the dashed line, indicating that the dust grains towards NGC 1893 have higher polarization efficiency in comparison to the the general ISM.

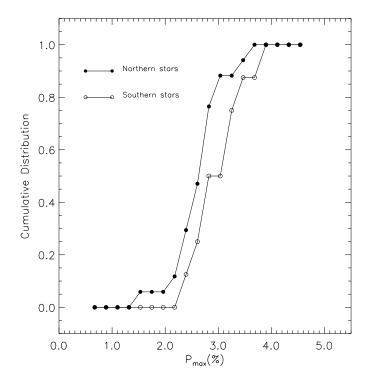


Figure 11. Cumulative distribution of  $P_{max}$  for the stars, with E(B-V) values between 0.4-0.6 mag, distributed in northern and southern parts of the cluster NGC 1893. The lines connecting filled and open circles are the cumulative distributions for northern and southern stars respectively.

### **4.4** Spatial variation of $P_{max}$ and E(B-V)

The upper panel of Fig. 10 shows  $P_{max}$  for the cluster members and the stars with uncertainty in their membership (# 108, 123, 196, 199 and 213), as a function of the radial distance from the ionization source (see Fig. 1: HD 242935; shown by the plus symbol). Stars located in the northern and southern parts of the cluster are shown by filled and open circles respectively. The distribution of  $P_{max}$  within a radial distance of  $\sim 5'$  from the ionization source shows a decreasing trend with the increase in radial distance. The distribution of  $P_{max}$  shown in Fig. 10 also reveal that  $P_{max}$  in the southern region is relatively higher than that of the northern region. There is a significant increase in the  $P_{max}$  values at  $\sim 5'.5$ . The increase in  $P_{max}$  is mainly due to the YSOs distributed around the nebulae Sim 129 and 130, located towards the North-East direction of HD 242935 at a radial distance of  $\sim 6'$ .

The lower panel of Fig. 10 shows radial variation of E(B-V). The distribution of E(B-V) reveals a clumpy nature of the gas/dust distribution. The polarization efficiency in the northern region of the cluster at a radial distance  $\sim 0.5$ , assuming a normal value of  $R_V=3.1$ , comes out to be  $\sim 6.0$ , and decreases to  $\sim 5.0$  at the boundary ( $\sim 4$ ) of the cluster. The ratio  $P_{max}/E(B-V)$  depends mainly on the alignment efficiency, magnetic strength

and amount of depolarization due to radiation traversing through more than one medium. The polarization efficiency  $P_{\lambda}/A_{\lambda}$  also depends on the particle shape (Voshchinnikov & Das 2008).

The weighted mean of  $P_{max}$  for stars having  $0.40 \leqslant E(B-V) \leqslant 0.60$  lying in the northern and southern regions of the cluster is estimated to be as  $2.64\pm0.04\%$  and  $2.77\pm0.07\%$ . Fig. 11 shows the cumulative distribution of  $P_{max}$  in both regions, for stars having  $0.40 \leqslant E(B-V) \leqslant 0.60$  mag, which indicates that  $P_{max}$  values in the southern region are systematically higher than those in the northern region. Kolmogorov-Smirnov test indicates that these distributions are different at 80% confidence level.

The weighted mean values of polarization angle  $(\theta_V)$  for northern and southern regions are  $161 \pm 4^{\circ}$  and  $162 \pm 6^{\circ}$ , which indicate that there is no difference in  $\theta_V$  in the two regions.

# 5 DUST COMPONENTS RESPONSIBLE FOR THE OBSERVED POLARIZATION

The degree of polarization of a star increases as a function of distance due to the presence of a column of aligned dust grains along the pencil beam of radiation from the star. The degree of polarization shows a sudden jump if the radiation from the stars encounter a dust layer located at a certain distance between the star and the observer. The number of such sudden jumps is characterized by the number of dust layers encountered by the radiation along its path and the relative magnetic field orientations in the dust layers.

To understand the distribution of dust layers towards the direction of NGC 1893, we selected stars from a region of 10° radius around the cluster with both polarization measurements (Heiles 2000) and Hipparcos parallaxes (van Leeuwen, 2007) available. In Fig. 12 we show the degree of polarization versus distance (upper panel) and polarization angle versus distance (lower panel) plots for the selected stars (filled circles). Stars observed towards the clusters NGC 2281, NGC 1664, NGC 1960, Stock 8 and NGC 1893 are also shown using inverted triangles, squares, triangles, open circles and star symbols respectively. Two significant jumps in the values of  $P_V$ , one at  $\sim 170$  pc and another at  $\sim 360$  pc, are clearly evident in the  $P_V$  versus distance plot (upper panel).

For distances  $\lesssim 170$  pc, the  $\theta_V$  values show a scattered distribution between  $\sim 50^{\circ} - 130^{\circ}$ . At  $\sim 170$  pc, the  $\theta_V$  values show a dip to  $\sim 20^{\circ}$ . A sharp rise in  $\theta_V$  values from  $\sim 20^{\circ}$  to  $160^{\circ}$  is evident at a distance of  $\sim 360$  pc. The stars located beyond  $\sim 1000$  pc show an average

polarization angle of  $\theta_V \sim 163^\circ$ . On the basis of Fig. 12, we infer that a dust layer at  $\sim 170$  pc contributes  $\sim 0.3-0.9\%$  to the polarization and the dust grains are aligned towards  $\theta_V \sim 20^\circ$ . Another dust layer with  $\theta_V \sim 160-170^\circ$  at a distance  $\sim 360$  pc further contributes  $\sim 0.3-1.3\%$  (i.e., total  $\sim 1.2$  to  $\sim 2.2$  %). The clusters located at distance  $\gtrsim 1000$  pc show  $P_V$  in the range of  $\sim 1-4\%$ . The  $P_V \gtrsim 2.2\%$  in these clusters must be due to intracluster medium. The optical properties derived in Sections 4.2 and 4.3 should be a combined effect of dust layers at d  $\sim 170$  pc,  $\sim 360$  pc and intracluster medium.

Neckel and Klare (1980) have studied  $A_V$  distribution in the Galactic plane with  $|b| \leq 7.6^{\circ}$  using extinction and distances computed for individual stars. The  $A_V$  map towards the direction of NGC 1893 by Neckel and Klare (1980) reveals that  $A_V$  increases with distance up to  $\sim 2$  kpc. Beyond  $\sim 2$  kpc  $A_V$  is found to be rather constant, indicating that the dust contribution in the distance range 2-3 kpc is negligible. Here, it is worthwhile to mention that the mean polarization  $P_V$  in the Stock 8 (2.4±0.6%) and NGC 1893 (2.6±0.7%) is almost the same, which further confirms that the contribution of dust in the distance range  $\sim 2$ -3 kpc is negligible. Further, the observed mean polarization values are consistent with the E(B-V) values mentioned in Table 1.

#### 6 CONCLUSIONS

We have made polarimetric observations of the open cluster NGC 1893 in B, V,  $R_c$  and  $I_c$  bands. Three additional open clusters towards the direction of NGC 1893, namely, NGC 2281, NGC 1960 and Stock 8 along with NGC 1664 toward anticenter direction of the Galaxy were observed in V-band only. The main aim of the study is to investigate the properties of dust grains towards the anticenter direction of the Galaxy between  $l \sim 160^{\circ}$  to  $\sim 175^{\circ}$ , using stars of open clusters located in the distance range of 600 pc (NGC 2281) to 3.2 kpc (NGC 1893).

The stars located at distances  $\leq 170$  pc show a large scatter in  $\theta_V$  values with a polarization of  $\sim 0.1\%$ . The degree of polarization is found to increase with the distance. The distribution of  $P_V$  and  $\theta_V$  as a function of distance reveals two dust layers at  $\sim 170$  pc and  $\sim 360$  pc. The first dust layer is characterized by its polarized components as  $P_V \sim 0.3-0.9\%$  and  $\theta_V \sim 20-50^\circ$ . Both dust layers produce a maximum combined polarization up to  $P_V \sim 2.2\%$ . Polarization values higher than the  $\sim 2.2\%$  should be due to intracluster medium.

The magnetic field orientation remains unchanged within the Galactic plane  $|b| < 2^{\circ}$ .

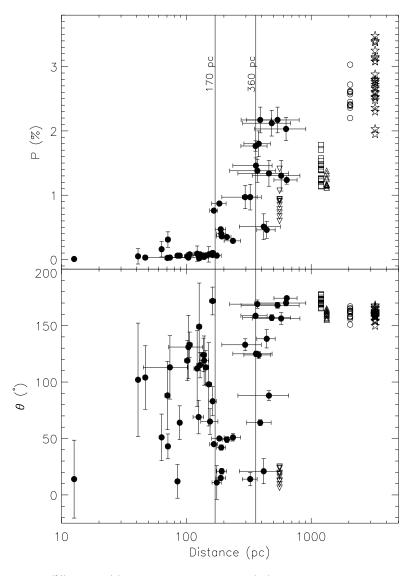


Figure 12. The change in  $P_V(\%)$  and  $\theta_V(^\circ)$  as a function of distance (pc) is plotted in the upper and lower panels for stars (filled circles) selected from a circular region of  $10^\circ$  around NGC 1893. The P% and  $\theta^\circ$  values are obtained from the Heiles (2000) catalog and the distances are obtained from Hipparcos parallaxes (van Leeuwen, 2007). The vertical solid lines are drawn at 170 pc and 360 pc. The results from our study of the five clusters are also shown. The clusters are represented by the same symbols as in Fig. 5.

The estimated mean value of the polarization angle (assuming a Gaussian distribution) of the four clusters (NGC 1664, NGC 1960, Stock 8 and NGC 1893) comes out to be  $\sim 163^{\circ}$  with a standard deviation of 6°. This small dispersion in polarization angle could be due to the presence of a uniform dust layer beyond 1 kpc. Present observations reveal that in case of NGC 1893, the foreground two dust layers, in addition to the intracluster medium, seems to be responsible for the polarization effects.

The estimated mean values of  $P_V$  for the two clusters namely, Stock 8 and NGC 1893, imply that the ISM located between 2-3 kpc distance has negligible contribution towards

extinction as well as the observed polarization. Present polarimetric results are consistent with the reddening distribution given by Neckel and Klare (1980).

The weighted mean of the  $P_{max}$  and  $\lambda_{max}$  values for NGC 1893 are found to be 2.59  $\pm$  0.02% and 0.55  $\pm$  0.01  $\mu$ m respectively. The estimated  $\lambda_{max}$  is quite similar to that of the general interstellar medium. The value of  $R_V$  using the relation  $R_V = 5.6 \times \lambda_{max}$  (Whittet & Van Breda 1978) is found to be close to the average value of 3.1 for the Milky Way Galaxy, implying that the average size of the dust grains within the cluster NGC 1893 is similar to the general interstellar medium. We also identified four candidate stars with intrinsic polarization in NGC 1893.

The radial distribution of  $P_{max}$  within the cluster shows a decrease of  $P_{max}$  towards the outer region of the cluster. The  $P_{max}$  and the polarization efficiency is found to be higher towards the southern region of the cluster. We have shown that the polarization measurements in combination with (U - B)/(B - V) colour-colour diagram provide a good tool to determine the membership in a cluster.

#### ACKNOWLEDGMENTS

Authors are thankful to the anonymous referee for useful comments which improved the scientific content and presentation of the paper. This publication makes use of data from the 2MASS (a joint project of the University of Massachusetts and the Infrared Processing and Analysis Center /California Institute of Technology, funded by the National Aeronautics and Space Administration and the National Science Foundation). This research has made use of the WEBDA database, operated at the Institute for Astronomy of the University of Vienna, as well as has used the images from the Digital Sky Survey (DSS), which was produced at the Space Telescope Science Institute under the US Government grant NAG W-2166. We have also used NASA's Astrophysics Data System and RAF, distributed by National Optical Astronomy Observatories, USA.

#### REFERENCES

Aannestad P. A., Purcell E, M., 1973, ARA&A, 11, 309

Bessell M. S., Brett J. M., 1988, PASP, 100, 1134

Boden E., 1951, UppAn, 3, 1

Carpenter J. M., 2001, AJ, 121, 2851

Cho J., Lazarian A., 2005, ApJ, 631, 361

Cohen J. G., Persson S. E., Elias J. H., Frogel J. A., 1981, ApJ, 249, 481

Coyne G. V., 1974, AJ, 79, 565

Coyne G. V., Gehrels T., Serkowski K., 1974, AJ, 79, 581

Cuffey J., Shapley H., 1937, AnHar, 105, 403

Cutri R. M., et al. 2003, The IRSA 2MASS All-Sky Point Source Catalog, NASA/IPAC

Infrared Science Archive (http://irsa.ipac.caltech.edu/applications/Gator/)

Davis L. Jr., Greenstein J. L., 1951, ApJ, 114, 206

Dias W. S., Assafin M., Flório V., Alessi B. S., Líbero V., 2006, A&A, 446, 949

Dolginov A. Z., 1990, IAUS, 140, 242

Dougherty S. M., Waters L. B. F. M., Burki G., Cote J., Cramer N., van Kerkwijk M. H.,

Taylor A. R., 1994, A&A, 290, 609

Feinstein C., Baume G., Vázquez R., Niemela V., Cerruti M. A., 2000, AJ, 120, 1906

Feinstein C., Baume G., Vergne M. M., Vázquez R., 2003, A&A, 409, 933

Feinstein C., Martínez R., Vergne M. M., Baume G., Vázquez R., 2003, ApJ, 598, 349

Feinstein C., Vergne M. M., Martínez R., Orsatti A. M., 2008, 391, 447

Fosalba P., Lazarian A., Prunet S., Tauber J. A., 2002, ApJ, 564, 762

Girardi L., Bertelli G., Bressan A., Chiosi C., Groenewegen M. A. T., Marigo P., Salasnich

B., Weiss A., 2002, A&A, 391, 195

Glaspey J. W., 1987, PASP, 99, 1089

Haikala L. K., 1995, A&A, 294, 89.

Heiles C., 2000, AJ, 119, 923

Hernández J., Calvet N., Hartmann L., Briceño C., Sicilia-Aguilar A., Berlind P., 2005,

AJ, 129, 856

Hoag A. A., Johnson H. L., Iriarte B., Mitchell R. I., Hallam K. L., Sharpless S., 1961,

Publ. Us. Nav. Obs. XVII part VII, 347

Hoag A. A., Johnson H. L., Iriarte B., Mitchell R. I., Hallam K. L., Sharpless S., 1961,

PUSNO, 17, 347

Johnson H. L., Morgan W. W., 1953, ApJ, 117, 313

Jose J., Pandey A. K., Ojha D. K., Ogura K., Chen W. P., Bhatt B. C., Ghosh S. K., Mito

H., Maheswar G., Sharma S., 2008, MNRAS, 384, 1675

Kharchenko N. V., Piskunov A. E., Röser S., Schilbach E., Scholz R.-D., 2005, A&A, 438,

1163

Larsson-Leander G., 1957, StoAn, 20, 1

Marco A., Negueruela I., 2002, A&A, 393, 195

Marraco H. G., Vega E. I., Vrba F. J., 1993, AJ, 105, 258

Martin P. G., 1974, ApJ, 187, 461

Martínez R., Vergne M. M., Feinstein C., 2004, A&A, 419, 965

Massey P., Johnson K. E., Degioia-Eastwood K., 1995, ApJ, 454, 151

Mayer P., 1964, AcMPh, 1, 25

McMillan R. S., 1978, ApJ, 225, 880

Medhi B. J., Maheswar G., Brijesh K., Pandey J. C., Kumar T. S., Sagar R., 2007, MNRAS, 378, 881

Medhi B. J., Maheswar G., Pandey J. C., Kumar T. S., Sagar R., 2008, MNRAS, 388, 105

Medhi B J., Maheswar G., Pandey J. C., Tamura M., Sagar R., 2010, MNRAS, 403, 1577

Neckel Th., Klare G., 1980, A&AS, 42, 251

Negueruela I., Marco A., Israel G. L., Bernabeu G., 2007, A&A, 471, 485

Orsatti A. M., Feinstein C., Vega E. I., Vergne M. M., 2007, A&A, 471, 1650

Pandey J. C., Medhi B. J., Sagar R., Pandey A. K., 2009, MNRAS, 396, 1004

Pesch P., 1961, ApJ, 134, 602

Purcell E. M., 1979, ApJ, 231, 404

Purgathofer A., 1964, AnWie, 26, 37

Ramaprakash A. N., Gupta R., Sen A. K., Tandon S. N., 1998, A&AS, 128, 369

Rautela B. S., Joshi G. C., Pandey J. C., 2004, BASI, 32, 159

Schmidt G, D., Elston R., Lupie O. L., 1992, AJ, 104, 1563

Schmidt-Kaler Th., 1982, in Schaifers K., Voigt H. H., Landolt H., eds, Landolt-Bornstein,

Vol. 2b. Springer, Berlin, p. 19

Serkowski K., 1973, IAUS, 52, 145.

Serkowski K., Mathewson D. S., Ford V. L., 1975, ApJ, 196, 261

Sharma S., Pandey A. K., Ogura K., Mito H., Tarusawa K., Sagar R., 2006, AJ, 132, 1669

Sharma S., Pandey A. K., Ojha D. K., Chen W. P., Ghosh S. K., Bhatt B. C., Maheswar

G., Sagar R., 2007, MNRAS, 380, 1141

Siess L., Dufour E., Forestini M., 2000, A&A, 358, 593

van Leeuwen F., 2007, A&A, 474, 653

Vasilevskis S., Balz A. G. A., 1959, AJ, 64, 170

Vergne M. M., Feinstein C., Martínez R., 2007, A&A, 462, 621

Vergne M. M., Feinstein C., Martínez R., Orsatti A. M., Alvarez M. P., 2010, MNRAS, 403, 2041

Voshchinnikov N. V., Das H. K., 2008, J. Quant. Spectrosc. Radiative Transfer, 109, 1527

Wilking B. A., Lebofsky M. J., Rieke G. H., 1982, AJ, 87, 695

Whittet, D. C. B. 1992, Dust in the Galactic Environment (Philadelphia: Inst. Phys. Publ.)

Whittet D. C. B., van Breda I. G., 1978, A&A, 66, 57

Yoshizawa M., 1978, PASJ, 30, 123

 ${\bf Table~3.~Observed~polarized~and~unpolarized~standard~stars}$ 

	$P \pm \epsilon_P(\%)$ Our wor	$ heta \pm \epsilon_{ heta}(^{\circ})$ k	$P \pm \epsilon_P(\%)$ Schmidt et a	$\theta \pm \epsilon_{\theta}(^{\circ})$ al. (2002)				
			andard stars	(				
		2008 Nove	mber 8 & 9					
		•	59°389					
B	$6.32 \pm 0.22$	$97.9 \pm 1.0$	$6.34 \pm 0.04$	$98.14 \pm 0.16$				
V	$6.86 \pm 0.16$	$97.3 \pm 0.7$	$6.70 \pm 0.01$	$98.09 \pm 0.07$				
$R_c$	$6.43 \pm 0.13$	$96.0 \pm 0.6$	$6.43 \pm 0.02$	$98.14 \pm 0.10$				
$I_c$	$5.86 \pm 0.11$	97.0±0.5	$5.80 \pm 0.02$ $4^{\circ} 106$	$98.26 \pm 0.11$				
B	$5.73 \pm 0.21$	97.3±1.0	$5.51 \pm 0.09$	$97.15 \pm 0.47$				
V	$5.68 \pm 0.19$	$96.7\pm1.0$	$5.69 \pm 0.04$	$96.63\pm0.18$				
$R_c$	$5.08 \pm 0.19$ $5.12 \pm 0.17$	$97.4\pm0.9$	$5.09 \pm 0.04$ $5.15 \pm 0.10$	$96.74\pm0.54$				
$I_c$	$4.66 \pm 0.21$	$97.4\pm0.9$ $97.8\pm1.3$	$4.70 \pm 0.05$	$96.89 \pm 0.32$				
$I_C$	$4.00\pm 0.21$		4.70 ±0.05 4° <b>106</b>	90.69±0.32				
B	$5.65 \pm 0.22$	$97.4 \pm 1.1$	$5.51 \pm 0.09$	$97.15 \pm 0.47$				
V	$5.49 \pm 0.20$	$96.9\pm1.0$	$5.69 \pm 0.04$	$96.63\pm0.18$				
$R_c$	$5.49 \pm 0.20$ $5.33 \pm 0.18$	$95.8\pm0.9$	$5.09 \pm 0.04$ $5.15 \pm 0.10$	$96.74\pm0.54$				
$I_c$	$4.48 \pm 0.22$	$98.7 \pm 1.4$	$4.70 \pm 0.05$	$96.74\pm0.34$ $96.89\pm0.32$				
1 c	4.46± 0.22		4.70 ±0.05 04827	90.69±0.32				
B	$5.68 \pm 0.23$	58.0±1.2	$5.65 \pm 0.02$	$58.20 \pm 0.11$				
V	$5.47 \pm 0.17$	$59.1 \pm 0.8$	$5.32 \pm 0.01$	$58.73 \pm 0.08$				
$R_c$	$5.19 \pm 0.14$	$61.5 \pm 0.8$	$4.89 \pm 0.03$	$59.10\pm0.17$				
$I_c$	$4.02 \pm 0.11$	$58.5 \pm 1.2$	$4.19 \pm 0.03$	$59.94 \pm 0.20$				
10	1.021 0.10			00.0120.20				
2009 November 23								
B	$4.49 \pm 0.11$	$114.9 \pm 0.7$	$9820$ $4.699 \pm 0.036$	$115.70 \pm 0.22$				
V	$4.49 \pm 0.11$ $4.89 \pm 0.09$	$114.9 \pm 0.7$ $114.2 \pm 0.5$		$113.70 \pm 0.22$ $114.93 \pm 0.17$				
			$4.787 \pm 0.028$					
$R_c$	$4.49 \pm 0.09$	$115.5 \pm 0.6$ $115.3 \pm 1.0$	$4.526 \pm 0.025$ $4.081 \pm 0.024$	$114.46 \pm 0.16$ $114.48 \pm 0.17$				
$I_c$	$4.06 \pm 0.16$		$4.081 \pm 0.024$	114.46 ± 0.17				
B	$5.19 \pm 0.09$	$134.6 \pm 0.5$	$5.232 \pm 0.092$	$134.28 \pm 0.51$				
V	$5.04 \pm 0.07$	$136.0 \pm 0.4$	$5.127 \pm 0.061$	$134.23 \pm 0.34$				
$I_c$	$4.19 \pm 0.09$	$134.8 \pm 0.6$		$134.21 \pm 0.28$				
_		•	34°106					
B	$5.49 \pm 0.17$	$98.0 \pm 0.9$	$5.506 \pm 0.090$	$97.15 \pm 0.47$				
$R_c$	$5.41 \pm 0.11$	$96.1 \pm 0.6$	$5.150 \pm 0.098$	$96.74 \pm 0.54$				
$I_c$	$4.50 \pm 0.14$	$96.6 \pm 0.9$	$4.696 \pm 0.052$	$96.89 \pm 0.32$				
		2009 Dec	ember 24					
_			9820					
B	$4.72 \pm 0.11$	$115.6 \pm 0.7$	$4.699 \pm 0.036$	$115.70 \pm 0.22$				
V	$4.79 \pm 0.08$	$115.1 \pm 0.5$	$4.787 \pm 0.028$	$114.93 \pm 0.17$				
$R_c$	$4.51 \pm 0.07$	$114.6 \pm 0.4$	$4.526 \pm 0.025$	$114.46 \pm 0.16$				
$I_c$	$3.97 \pm 0.09$	$115.7 \pm 0.6$	$4.081 \pm 0.024$ <b>5443</b>	$114.48 \pm 0.17$				
B	$5.12 \pm 0.09$	$134.0 \pm 0.5$	$5.232 \pm 0.092$	$134.28 \pm 0.51$				
V	$5.12 \pm 0.09$ $5.27 \pm 0.09$	$134.8 \pm 0.5$	$5.127 \pm 0.061$	$134.23 \pm 0.31$ $134.23 \pm 0.34$				
$R_c$	$5.00 \pm 0.08$	$134.5 \pm 0.4$ $134.5 \pm 0.4$	$4.734 \pm 0.045$	$133.65 \pm 0.28$				
$I_c$	$4.19 \pm 0.07$	$136.0 \pm 0.5$	$4.249 \pm 0.041$	$134.21 \pm 0.28$				
10	1.10 ± 0.01			101.21 ± 0.20				
	DD + 6	32°3739	standard stars HD212	911				
	q (%)	u (%)	q (%)	u (%)				
	4 (70)		wrok	u (/0)				
В	0.089	-0.093	0.138	0.001				
	0.171	-0.058	-0.184	-0.043				
V	0.171	0.000						
$V \\ R_c$	-0.072	-0.078	0.042	0.016				

Table 4. Observed  $B, V, (RI)_c$  polarization and polarization angles for stars towards NGC 1893

$\operatorname{Id}^{\dagger}$	V (mag) <sup>‡</sup>	$P_B \pm \epsilon(\%)$	$\theta_B \pm \epsilon$ (°)	$P_V \pm \epsilon(\%)$	$\theta_V \pm \epsilon$ (°)	$P_{Rc} \pm \epsilon (\%)$	$\theta_{Rc} \pm \epsilon (^{\circ})$	$P_{Ic} \pm \epsilon (\%)$	$\theta_{Ic} \pm \epsilon (^{\circ})$
(1)	(2)	(3)	(4)	(5)	(6)	(7)	(8)	(9)	(10)
1	10.19	$2.35 \pm 0.14$	$160.3 \pm 1.6$	$2.52 \pm 0.14$	$159.5 \pm 1.5$	$2.44 \pm 0.14$	$154.9 \pm 1.5$	$1.93 \pm 0.18$	$155.6 \pm 2.5$
2	11.29	$2.90 \pm 0.23$	$157.0 \pm 2.1$	$3.15 \pm 0.24$	$160.8 \pm 1.9$	$3.06 \pm 0.22$	$156.6 \pm 2.0$	$2.38 \pm 0.29$	$164.4 \pm 3.4$
3	11.16	$2.31 \pm 0.16$	$157.3 \pm 1.9$	$2.30 \pm 0.15$	$163.1 \pm 1.8$	$2.27 \pm 0.15$	$162.1 \pm 1.9$	$2.28 \pm 0.18$	$159.1 \pm 2.2$
5	13.41	$2.22 \pm 0.46$	$156.8 \pm 5.6$	$2.79 \pm 0.42$	$158.0 \pm 4.1$	$2.30 \pm 0.41$	$155.5 \pm 5.0$	$1.95 \pm 0.47$	$151.7 \pm 6.6$
9	12.71	$2.54 \pm 0.34$	$160.8 \pm 3.7$	$2.76 \pm 0.31$	$165.7 \pm 3.0$	$2.87 \pm 0.29$	$162.9 \pm 2.8$	$2.03 \pm 0.32$	$156.2 \pm 4.3$
10	13.69	$2.15 \pm 0.24$	$161.9 \pm 3.1$	$2.03 \pm 0.23$	$157.2 \pm 3.0$	$2.28 \pm 0.23$	$162.9 \pm 2.7$	$2.10 \pm 0.26$	$158.6 \pm 3.3$
13	12.46	$2.28 \pm 0.52$	$153.3 \pm 6.3$	$1.95 \pm 0.46$	$157.4 \pm 6.3$	$3.01 \pm 0.44$	$157.9 \pm 4.0$	$2.38 \pm 0.45$	$161.8 \pm 5.3$
15	13.02	$2.66 \pm 0.42$	$156.4 \pm 4.2$	$3.08 \pm 0.48$	$165.8 \pm 3.7$	$2.43 \pm 0.44$	$161.9 \pm 4.9$	$2.90 \pm 0.54$	$162.6 \pm 5.2$
33	12.27	$2.11 \pm 0.35$	$161.9 \pm 4.3$	$2.52 \pm 0.38$	$168.0 \pm 3.5$	$2.04 \pm 0.34$	$159.2 \pm 4.5$	$2.15 \pm 0.44$	$160.2 \pm 5.6$
48 59	11.01 $12.10$	$1.83 \pm 0.27$ $2.32 \pm 0.38$	$166.0 \pm 4.0$ $156.8 \pm 4.4$	$1.81 \pm 0.19$ $2.79 \pm 0.40$	$165.6 \pm 2.7$ $159.6 \pm 3.6$	$1.32 \pm 0.18$ $2.95 \pm 0.36$	$164.2 \pm 3.7$ $155.4 \pm 3.4$	$1.59 \pm 0.17$ $2.38 \pm 0.46$	$165.2 \pm 2.9$ $161.6 \pm 5.3$
62	12.10	$2.32 \pm 0.38$ $2.06 \pm 0.31$	$162.8 \pm 4.4$ $162.8 \pm 4.2$	$2.79 \pm 0.40$ $2.59 \pm 0.29$	$159.0 \pm 3.0$ $159.3 \pm 3.0$	$2.93 \pm 0.30$ $2.44 \pm 0.27$	$153.4 \pm 3.4$ $158.0 \pm 3.1$	$1.91 \pm 0.29$	$163.9 \pm 4.2$
72	12.53	$1.40 \pm 0.43$	$172.4 \pm 8.2$	$1.16 \pm 0.31$	$174.7 \pm 7.2$	$1.87 \pm 0.34$	$162.0 \pm 5.0$	$1.81 \pm 0.29$ $1.81 \pm 0.39$	$162.2 \pm 5.8$
73	10.77	$1.66 \pm 0.18$	$169.2 \pm 2.7$	$1.89 \pm 0.19$	$169.2 \pm 2.3$	$1.72 \pm 0.01$	$167.8 \pm 2.7$	$1.36 \pm 0.33$ $1.36 \pm 0.23$	$173.9 \pm 4.5$
82	12.94	$2.67 \pm 0.52$	$154.5 \pm 5.2$	$3.25 \pm 0.48$	$153.8 \pm 4.1$	$3.56 \pm 0.44$	$150.4 \pm 3.4$	$2.82 \pm 0.53$	$165.3 \pm 5.2$
92	11.72	$1.27 \pm 0.26$	$169.5 \pm 5.5$	$1.54 \pm 0.25$	$162.3 \pm 4.2$	$1.47 \pm 0.30$	$160.5 \pm 5.5$	$1.28 \pm 0.34$	$158.4 \pm 7.1$
98	13.28	$3.67 \pm 0.56$	$158.9 \pm 4.3$	$3.40 \pm 0.51$	$157.3 \pm 4.1$	$2.96 \pm 0.58$	$157.3 \pm 5.4$	$3.05 \pm 0.60$	$165.1 \pm 5.4$
106	12.32	$2.97 \pm 0.29$	$160.3 \pm 2.7$	$2.66 \pm 0.26$	$159.0 \pm 2.7$	$2.64 \pm 0.25$	$159.4 \pm 2.6$	$2.54 \pm 0.28$	$162.7 \pm 3.0$
108	13.88	$2.55 \pm 0.59$	$154.8 \pm 6.4$	$3.67 \pm 0.54$	$159.3 \pm 4.0$	$2.94 \pm 0.52$	$165.9 \pm 4.9$	$2.26 \pm 0.58$	$157.9 \pm 7.0$
115	13.66	$2.72 \pm 0.48$	$162.4 \pm 4.9$	$2.80 \pm 0.43$	$160.3 \pm 4.1$	$2.98 \pm 0.40$	$163.0 \pm 3.8$	$2.36 \pm 0.43$	$158.3 \pm 4.9$
123	$13.23^{a}$	$3.65 \pm 0.42$	$163.6 \pm 3.2$	$3.57 \pm 0.40$	$160.9 \pm 3.0$	$4.04 \pm 0.39$	$157.3 \pm 2.7$	$2.31 \pm 0.42$	$158.1 \pm 5.0$
134	13.09	$2.91 \pm 0.40$	$160.4 \pm 3.8$	$3.38 \pm 0.38$	$167.1 \pm 3.0$	$2.74 \pm 0.37$	$155.2 \pm 3.7$	$3.07 \pm 0.41$	$164.6 \pm 3.7$
139	11.98	$2.20 \pm 0.27$	$161.4 \pm 3.3$	$2.76 \pm 0.25$	$160.4 \pm 2.5$	$2.82 \pm 0.31$	$160.5 \pm 3.1$	$2.46 \pm 0.42$	$160.6 \pm 4.7$
140	12.39	$2.65 \pm 0.33$	$165.1 \pm 3.4$	$2.48 \pm 0.30$	$158.5 \pm 3.3$	$2.87 \pm 0.37$	$157.9 \pm 3.6$	$2.30 \pm 0.49$	$154.9 \pm 5.8$
141	11.45	$2.49 \pm 0.23$	$164.3 \pm 2.4$	$2.53 \pm 0.25$	$160.1 \pm 2.5$	$2.40 \pm 0.23$	$157.9 \pm 2.7$	$2.48 \pm 0.31$	$162.6 \pm 3.5$
149	10.14	$2.69 \pm 0.13$	$157.2 \pm 1.3$	$2.68 \pm 0.11$	$149.8 \pm 1.1$	$2.87 \pm 0.12$	$149.9 \pm 1.2$	$2.33 \pm 0.15$	$144.4 \pm 1.7$
168	12.25	$2.12 \pm 0.33$	$160.1 \pm 4.3$	$2.36 \pm 0.32$	$154.3 \pm 3.7$	$2.01 \pm 0.40$	$146.8 \pm 5.4$	$2.36 \pm 0.44$	$152.6 \pm 5.1$
$\frac{196}{197}$	$12.33^a$ $11.87$	$1.82 \pm 0.33$ $2.33 \pm 0.35$	$164.4 \pm 4.9$ $162.4 \pm 4.1$	$2.45 \pm 0.29$ $2.13 \pm 0.22$	$159.7 \pm 3.1$ $161.3 \pm 2.7$	$2.17 \pm 0.25$ $1.99 \pm 0.16$	$164.5 \pm 3.1$ $163.3 \pm 2.2$	$2.07 \pm 0.26$ $2.00 \pm 0.14$	$167.8 \pm 3.4$ $164.7 \pm 1.9$
199	13.40	$1.82 \pm 0.46$	$157.3 \pm 6.8$	$3.77 \pm 0.40$	$151.3 \pm 2.7$ $154.9 \pm 2.9$	$2.59 \pm 0.10$ $2.59 \pm 0.37$	$105.3 \pm 2.2$ $146.2 \pm 3.9$	$2.00 \pm 0.14$ $2.16 \pm 0.36$	$104.7 \pm 1.9$ $148.2 \pm 4.6$
209	$12.63^a$	$2.72 \pm 0.40$	$165.7 \pm 3.0$	$1.80 \pm 0.29$	$168.2 \pm 4.2$	$1.84 \pm 0.29$	$167.9 \pm 4.3$	$1.79 \pm 0.34$	$163.4 \pm 5.2$
213	14.52	$2.98 \pm 0.78$	$143.6 \pm 7.2$	$3.99 \pm 0.69$	$165.2 \pm 4.7$	$2.72 \pm 0.62$	$159.7 \pm 6.3$	$2.84 \pm 0.64$	$173.6 \pm 6.2$
215	14.23	$3.42 \pm 0.69$	$156.8 \pm 5.6$	$2.72 \pm 0.63$	$164.8 \pm 6.1$	$2.55 \pm 0.58$	$157.7 \pm 6.3$	$2.02 \pm 0.62$	$154.4 \pm 8.4$
219	13.97	$3.82 \pm 0.63$	$156.7 \pm 4.6$	$3.38 \pm 0.56$	$161.8 \pm 4.4$	$4.12 \pm 0.51$	$155.0 \pm 3.5$	$2.67 \pm 0.55$	$159.5 \pm 5.6$
222	14.16	$2.32 \pm 0.65$	$169.0 \pm 7.6$	$2.61 \pm 0.60$	$154.7 \pm 6.3$	$2.33 \pm 0.59$	$164.4 \pm 6.9$	$2.31 \pm 0.66$	$164.0 \pm 7.9$
228	12.50	$2.12 \pm 0.35$	$162.0 \pm 4.5$	$3.13 \pm 0.32$	$162.6 \pm 2.8$	$2.71 \pm 0.39$	$155.7 \pm 4.0$	$2.37 \pm 0.50$	$158.8 \pm 5.9$
301	$10.94^{a}$	$3.16 \pm 0.13$	$160.0 \pm 1.2$	$3.08 \pm 0.13$	$160.9 \pm 1.2$	$2.92 \pm 0.13$	$161.9 \pm 1.3$	$2.96 \pm 0.16$	$162.5 \pm 1.4$
307	$11.68^{a}$	$3.14 \pm 0.19$	$159.7 \pm 1.7$	$3.48 \pm 0.19$	$159.9 \pm 1.5$	$3.33 \pm 0.19$	$159.3 \pm 1.6$	$3.02 \pm 0.22$	$158.8 \pm 2.0$
310	$12.59^{a}$	$2.33 \pm 0.42$	$160.4 \pm 4.9$	$2.00 \pm 0.29$	$167.6 \pm 3.8$	$1.71 \pm 0.23$	$166.9 \pm 3.6$	$1.53 \pm 0.21$	$163.6 \pm 3.7$
320	$12.43^{a}$	$2.59 \pm 0.29$	$164.7 \pm 3.1$	$2.88 \pm 0.29$	$161.6 \pm 2.8$	$2.65 \pm 0.36$	$165.8 \pm 3.7$	$2.38 \pm 0.46$	$160.6 \pm 5.3$
327	$11.62^{a}$	$1.25 \pm 0.22$	$161.7 \pm 4.7$	$1.01 \pm 0.21$	$164.3 \pm 5.3$	$1.06 \pm 0.26$	$156.0 \pm 6.5$	$1.05 \pm 0.34$	$168.4 \pm 8.5$
329	$11.95^a$	$1.20 \pm 0.26$	$152.7 \pm 5.7$	$0.84 \pm 0.24$	$160.5 \pm 7.4$	$1.03 \pm 0.32$	$148.4 \pm 8.0$	$1.49 \pm 0.42$	$164.5 \pm 7.6$
355	$13.46^a$	$1.61 \pm 0.53$	$154.8 \pm 8.8$	$1.94 \pm 0.47$	$168.2 \pm 6.6$	$2.01 \pm 0.53$	$168.7 \pm 7.2$	$2.01 \pm 0.64$	$170.8 \pm 8.6$
356	$14.35^{a}$	$2.57 \pm 0.80$	$160.7 \pm 8.6$	$2.01 \pm 0.67$	$164.0 \pm 8.7$	$3.23 \pm 0.58$	$157.3 \pm 5.0$	$1.85 \pm 0.60$	$150.6 \pm 8.7$

<sup>†:</sup> Cuffey and Shapley (1937) ‡: Sharma et al. (2007) a: Massey et al. (1995)

 $\textbf{Table 5.} \ \ \text{Polarimetric results for } 14 \ \text{stars observed towards NGC } 2281.$ 

Id.†	α(°)	δ(°)	V	$(B - V)^*$	$(U - B)^*$	$P_V$	$\theta_V$	$\mathcal{M}_p^{\dagger\dagger}$	$M_p^{\dagger\dagger\dagger}$
(1)	(J2000) (2)	(J2000) (3)	$(\text{mag})^*$ $(4)$	(5)	(6)	(%) (7)	(°) (8)	(9)	(10)
49	102.03038	41.077494	10.56	0.24	0.16	$1.07 \pm 0.17$	$16.16 \pm 4.28$	M	M (99)
53	102.06064	41.112788	11.02	0.33	0.13	$0.91 \pm\ 0.22$	$19.52 \pm 6.14$	M	M (99)
55	102.06337	41.073019	8.89	0.98	0.69	$1.00 \pm 0.08$	$13.77 \pm 2.10$	NM	M (99)
56	102.06596	41.095871	11.43	1.24	1.19	$1.04 \pm\ 0.25$	$6.23 \pm 6.39$	NM	NM (00)
57	102.07032	41.130267	10.61	0.23	0.15	$0.90 \pm 0.18$	$6.39 \pm 5.05$	M	M(99)
58	102.07208	41.083118	9.45	0.12	0.06	$0.73 \pm 0.10$	$9.65 \pm 3.53$	M	M(99)
60	102.08048	41.041193	12.71	0.56	0.07	$1.41 \pm 0.45$	$12.29 \pm 8.47$	M	M(99)
71	102.11072	41.024925	11.16	0.53	0.05	$0.78 \pm 0.23$	$24.01 \pm 7.43$	M	NM (00)
74	102.1166	41.081101	9.54	1.10	1.03	$0.56 \pm 0.11$	$22.08 \pm 4.62$	NM	NM (00)
78	102.13344	41.108674	10.63	0.22	0.15	$0.60 \pm 0.18$	$23.54 \pm 7.22$	M	M(99)
79	102.14759	41.090775	10.30	0.17	0.11	$0.67 \pm\ 0.15$	$12.83 \pm 5.60$	M	M(99)
82	102.15634	41.10563	10.08	0.14	0.10	$0.85 \pm\ 0.14$	$18.06 \pm 4.11$	M	M(99)
86	102.17038	41.066299	8.62	0.22	0.15	$0.93 \pm 0.07$	$19.43 \pm 1.92$	M	M (99)
91	102.18262	41.086379	11.41	0.35	0.12	$0.94 \pm\ 0.25$	$25.04 \pm 6.97$	M	M (99)

<sup>†:</sup> Vasilevskis & Balz (1959)

<sup>\*:</sup> Pesch (1961) except star no # 60 for which V magnitude, (B-V) and (U-B) colours are taken from Yoshizawa (1978) ††: Present Work †††: Vasilevskis & Balz (1959)

 ${\bf Table~6.~Polarimetric~results~on~27~stars~observed~towards~NGC~1664.}$ 

Id.†	$\alpha(^{\circ})$	δ(°)	V	(B-V)	(U-B)	$P_V$	$\theta_V$	$M_p$ ††	$M_p$ †††
	(J2000)	(J2000)	(mag)			(%)	(°)		
(1)	(2)	(3)	(4)	(5)	(6)	(7)	(8)	(9)	(10)
1	72.783342	43.665161	$13.50^{a}$	$1.61^{a}$	$1.68^{a}$	$2.44 \pm 0.35$	$165 \pm 4$	NM	-
4	72.769500	43.671624	$11.75^{b}$	$0.32^{b}$	$0.25^{b}$	$1.41 \pm 0.15$	$178 \pm 3$	M	M(65)
7	72.824534	43.671985	$12.25^{a}$	$0.30^{a}$	$0.24^{a}$	$1.14 \pm 0.18$	$165 \pm 4$	$\mathbf{M}$	M(89)
9	72.814747	43.680135	-	-	-	$2.75 \pm 0.14$	$164 \pm 1$	NM	-
12	72.749866	43.684928	$13.01^{a}$	$0.24^{a}$	$0.31^{a}$	$1.25 \pm 0.27$	$170 \pm 6$	$\mathbf{M}$	M(92)
13	72.760895	43.676324	$14.36^{b}$	$1.09^{b}$	$0.71^{b}$	$2.59 \pm 0.49$	$163 \pm 5$	NM	-
14	72.750261	43.676335	$12.79^{a}$	$0.51^{a}$	$0.28^{a}$	$1.25 \pm 0.26$	$170 \pm 5$	$\mathbf{M}$	M(91)
21	72.771228	43.648455	$11.81^{b}$	$0.29^{b}$	$0.26^{b}$	$1.39 \pm 0.15$	$173 \pm 3$	$\mathbf{M}$	M (82)
22	72.779262	43.640397	$14.00^{a}$	$0.54^{a}$	$0.38^{a}$	$2.33 \pm 0.42$	$171 \pm 5$	NM	M (86)
27	72.816757	43.656291	$13.87^{b}$	$0.51^{b}$	$0.21^{b}$	$2.10 \pm 0.39$	$175 \pm 5$	NM	NM (35)
35	72.804006	43.700468	$12.50^{c}$	$0.37^{c}$	$0.25^{c}$	$1.15 \pm 0.21$	$170 \pm 5$	$\mathbf{M}$	M (91)
37	72.790902	43.708346	$10.93^{b}$	$0.34^{b}$	$0.34^{b}$	$1.24 \pm 0.10$	$174 \pm 2$	$\mathbf{M}$	M (90)
47	72.754574	43.703638	-	-	-	$3.18 \pm 0.54$	$160 \pm 5$	NM	-
55	72.724155	43.662572	$11.06^{b}$	$1.23^{b}$	$1.00^{b}$	$1.71 \pm 0.11$	$169 \pm 2$	$\mathbf{M}$	M(71)
56	72.737611	43.657761	$12.66^{b}$	$0.35^{b}$	$0.26^{b}$	$1.40 \pm 0.23$	$177\pm4$	$\mathbf{M}$	M (91)
67	72.857380	43.672892	-	-	-	$1.21 \pm 0.38$	$171 \pm 8$	$\mathbf{M}$	M(92)
68	72.849878	43.675125	-	-	-	$1.57 \pm 0.27$	$168 \pm 5$	$\mathbf{M}$	M (87)
75	72.832061	43.704486	$11.25^{a}$	$1.06^{a}$	$0.83^{a}$	$1.47 \pm 0.13$	$173 \pm 2$	$\mathbf{M}$	M (92)
76	72.823740	43.720916	-	-	-	$1.53 \pm 0.36$	$177 \pm 6$	$\mathbf{M}$	M (87)
77	72.814271	43.709793	$12.84^{c}$	$0.49^{c}$	$0.25^{c}$	$1.40 \pm 0.25$	$174 \pm 5$	$\mathbf{M}$	M (65)
79	72.765348	43.727229	$13.75^{a}$	$0.54^{a}$	$0.50^{a}$	$2.06 \pm 0.38$	$165 \pm 5$	NM	-
87	72.700196	43.654016	-	-	-	$4.09 \pm 0.80$	$171 \pm 5$	NM	-
90	72.712849	43.643313	$13.03^{a}$	$0.51^{a}$	$0.30^{a}$	$1.47 \pm 0.29$	$170 \pm 5$	M	NM (17)
113	72.735822	43.721862	$12.97^{a}$	$0.53^{a}$	$0.27^{a}$	$1.45 \pm 0.29$	$175\pm5$	M	M (84)
154	72.780622	43.746898	-	-	-	$1.26 \pm 0.31$	$172 \pm 6$	M	- ′
158	72.719637	43.739690	$14.79^{a}$	$0.73^{a}$	$0.13^{a}$	$1.78 \pm 0.50$	$166 \pm 7$	M	_
164	72.691065	43.720635			-	$0.97 \pm 0.27$	$26\pm7$	NM	NM (00)

 $<sup>^{\</sup>dagger} :$  Larsson-Leander (1957)

a: Hoag et al. (1961) Publ. Us. Nav. Obs. XVII part VII, 347
b: Purgathofer (1964)
c: Hoag et al. (1961)
††: Present Work

 $<sup>^{\</sup>dagger\dagger\dagger}:$  Dias et al. (2006)

Table 7. Polarimetric results on 15 stars observed towards NGC 1960.

Id.†	$\alpha(^{\circ})$	δ(°)	V	$(B - V)^*$	$(U - B)^*$	$P_V$	$\theta_V$	$M_p$ ††	$M_p$ †††
(1)	(J2000) (2)	(J2000) (3)	$(mag)^*$ $(4)$	(5)	(6)	(%) (7)	(°) (8)	(9)	(10)
13	84.063492	34.120250	10.78	0.12	-0.26	$1.12 \pm 0.17$	$160 \pm 4$	M	M (94)
16	84.065508	34.143746	$8.86^{a}$	$-0.00^{a}$	$-0.66^{-a}$	$1.17 \pm 0.07$	$159 \pm 2$	M	M (94)
17	84.060257	34.139917	12.40	0.25	0.18	$1.16 \pm 0.35$	$162\pm8$	M	M (94)
23	84.095740	34.175955	$8.96^{a}$	$0.01^{a}$	-0.68 $^a$	$1.12 \pm 0.07$	$162\pm2$	M	M (94)
33	84.118160	34.122944	11.85	0.12	-0.07	$1.15 \pm 0.27$	$155 \pm 6$	M	M (94)
38	84.099176	34.099402	$9.92^{a}$	$0.05^{a}$	$-0.49^a$	$1.17 \pm 0.11$	$156 \pm 2$	M	M (94)
41	84.083418	34.103419	12.37	0.19	0.14	$1.28 \pm 0.35$	$160 \pm 7$	M	M (94)
44	84.047893	34.118557	11.35	0.09	-0.36	$1.38 \pm 0.22$	$163 \pm 4$	M	M (94)
55	84.081130	34.204218	11.61	0.10	-0.31	$1.44 \pm 0.24$	$147 \pm 5$	NM	M (94)
56	84.087224	34.211974	12.39	0.46	0.35	$1.15 \pm 0.26$	$157 \pm 6$	M	M (93)
61	84.132976	34.179480	$9.14^{a}$	$0.01^{a}$	$-0.66^a$	$0.81 \pm 0.08$	$155\pm2$	NM	M (94)
77	84.069337	34.083562	12.10	0.17	0.06	$1.50 \pm 0.31$	$162 \pm 6$	NM	M (94)
87	83.996719	34.174535	10.62	0.07	0.95	$1.34 \pm 0.16$	$161\pm3$	M	M (94)
91	84.040637	34.193293	10.34	0.01	-0.50	$1.25\pm0.14$	$165 \pm 3$	M	M (94)
92	84.024453	34.201113	10.93	0.03	-0.49	$1.16 \pm 0.18$	$164\pm4$	M	M (94)

<sup>†:</sup> Boden (1951)

Table 8. Polarimetric results on 21 stars observed towards Stock 8.

$\mathrm{Id}.^\dagger$	$\alpha(^{\circ})$	$\delta(^{\circ})$	V	(B - V)(*)	(U - B)(*)	$P_V$	$\theta_V$	$M_p^{\dagger\dagger}$	$M_p^{\dagger\dagger\dagger}$
	(J2000)	(J2000)	$(mag)^*$			(%)	(°)		
(1)	(2)	(3)	(4)	(5)	(6)	(7)	(8)	(9)	(10)
11	82.004547	34.450581	11.50	0.13	0.17	$1.57 \pm 0.14$	$163 \pm 2$	NM	M (66)
12	82.009061	34.404500	11.76	-0.36	0.28	$2.41 \pm 0.15$	$165 \pm 2$	M	M(66)
13	82.018190	34.489546	11.71	-0.47	0.30	$2.45 \pm 0.15$	$167 \pm 2$	M	M(64)
16	82.038176	34.473935	11.89	-0.40	0.29	$2.41 \pm 0.16$	$151\pm2$	M	M(65)
19	82.058027	34.438897	13.01	1.22	1.40	$2.17 \pm 0.28$	$157 \pm 4$	NM	M(77)
141	82.082569	34.420441	12.19	-0.24	0.51	$2.60 \pm 0.19$	$165 \pm 2$	M	M(57)
160	82.002940	34.493490	12.63	0.15	0.60	$1.62 \pm 0.23$	$163 \pm 4$	NM	NM (02)
173	82.082563	34.455984	12.81	0.37	0.31	$1.60 \pm 0.25$	$159 \pm 4$	NM	NM (47)
181	82.064303	34.423842	12.87	-0.32	0.33	$2.39 \pm 0.25$	$158 \pm 3$	M	M(68)
208	82.040118	34.446178	13.18	-0.14	0.30	$2.62 \pm 0.28$	$162 \pm 3$	M	M(74)
211	81.996346	34.444053	13.21	0.17	0.28	$1.93 \pm 0.30$	$159 \pm 4$	NM	NM (19)
218	82.004829	34.385705	13.29	-0.02	0.34	$2.61 \pm 0.31$	$162 \pm 3$	M	NM (43)
231	82.028692	34.394823	13.36	-0.14	0.31	$3.03 \pm 0.33$	$157 \pm 3$	M	M(72)
258	81.969263	34.389477	13.53	0.24	0.68	$2.57 \pm 0.35$	$161 \pm 4$	M	NM (00)
275	82.090470	34.409075	13.69	-0.17	0.62	$2.37 \pm 0.39$	$136 \pm 5$	?	-
294	82.003915	34.403745	13.81	0.38	0.46	$2.72 \pm 0.40$	$163 \pm 4$	M	M(52)
320	81.993454	34.470836	13.93	0.27	0.62	$2.20 \pm 0.45$	$156 \pm 6$	M	NM (01)
325	81.962444	34.428255	13.96	-0.08	0.82	$4.18 \pm 0.44$	$165 \pm 3$	?	M (71)
333	82.066055	34.399693	14.00	0.32	0.59	$2.40 \pm 0.45$	$163 \pm 5$	M	-
365	82.001149	34.457243	14.18	0.37	0.41	$2.17 \pm 0.46$	$165 \pm 6$	NM	-
425	81.991192	34.498474	14.39	0.19	0.55	$2.36 \pm 0.61$	$158\pm7$	M	NM (04)

<sup>†:</sup> Mayer (1964)

<sup>\*:</sup> Sharma et al. (2006)

<sup>&</sup>lt;sup>a</sup>: Johnson H.L., Morgan W.W. (1953)

<sup>††:</sup> Present Work

 $<sup>^{\</sup>dagger\dagger\dagger} :$  Dias et al. (2006)

<sup>\*:</sup> Jose et al. (2008) ††: Present Work

 $<sup>^{\</sup>dagger\dagger\dagger}:$  Dias et al. (2006)

**Table 9.** The  $P_{max}, \lambda_{max}, \sigma_1$  &  $\overline{\epsilon}$  for the observed 44 stars towards NGC 1893

Id.†	$\frac{E(B-V)^{\ddagger}}{(\text{mag})}$	α (°) (J2000)	δ (°) (J2000)	$P_{max} \pm \epsilon$ (%)	$\lambda_{max} \pm \epsilon \ (\mu m)$	$\sigma_1$	$\overline{\epsilon}$	$M_P^{\dagger\dagger}$	$M_P^{\dagger\dagger\dagger}$
(1)	(1) (2)	(3)	(4)	(5)	(6)	(7)	(8)	(9)	(10)
1	0.53	80.683340	33.440739	$2.50 \pm 0.08$	$0.53 \pm 0.04$	0.74	1.31	M	M (78)
2	0.54	80.686558	33.443501	$3.11 \pm 0.13$	$0.54 \pm 0.05$	0.69	1.23	$\mathbf{M}$	M(79)
3	0.45	80.706563	33.447926	$2.41 \pm 0.08$	$0.58 \pm 0.04$	0.91	1.38	$\mathbf{M}$	M (78)
5	0.46	80.725969	33.445042	$2.52 \pm 0.26$	$0.52 \pm 0.10$	0.59	0.47	$\mathbf{M}$	NM (9)
9	0.52	80.706864	33.425991	$2.76 \pm 0.18$	$0.53 \pm 0.07$	0.89	1.25	$\mathbf{M}$	M(75)
10	0.46	80.705199	33.428371	$2.61 \pm 0.28$	$0.70 \pm 0.14$	1.03	0.41	$\mathbf{M}$	NM(0)
13	0.52	80.692334	33.422447	$2.80 \pm 0.22$	$0.62 \pm 0.10$	0.54	0.54	M	M(79)
15	0.48	80.696872	33.418720	$2.89 \pm 0.25$	$0.57 \pm 0.10$	0.83	0.92	$\mathbf{M}$	M(61)
33	0.50	80.688066	33.406540	$2.32 \pm 0.20$	$0.56 \pm 0.10$	0.62	1.27	M	M(71)
48	$0.20^{a}$	80.699353	33.476135	$1.76 \pm 0.14$	$0.51 \pm 0.06$	1.46	0.17	NM	M(60)
59	0.47	80.741815	33.443459	$2.26 \pm 0.13$	$0.60 \pm 0.07$	0.72	0.98	$\mathbf{M}$	M(79)
62	0.47	80.739711	33.433380	$2.41 \pm 0.16$	$0.56 \pm 0.07$	0.82	0.65	M	M(74)
72	$0.20^{a}$	80.699203	33.368629	$1.86 \pm 0.40$	$0.87 \pm 0.23$	0.82	1.05	NM	NM (27)
73	0.27	80.688608	33.371365	$1.80 \pm 0.11$	$0.53 \pm 0.06$	0.58	0.50	NM	M(79)
82	0.70	80.654111	33.386971	$3.32 \pm 0.26$	$0.63 \pm 0.10$	0.62	0.87	M	M(77)
92	0.44	80.668795	33.491486	$1.48 \pm 0.15$	$0.59 \pm 0.12$	0.31	0.58	NM	M(74)
98	0.68	80.722431	33.509064	$3.55 \pm 0.35$	$0.50 \pm 0.09$	0.56	0.49	$\mathbf{M}$	NM (3)
106	0.52	80.751932	33.496628	$2.87 \pm 0.16$	$0.53 \pm 0.06$	0.90	0.49	$\mathbf{M}$	M(74)
108	0.46	80.765402	33.487503	$3.13 \pm 0.34$	$0.52 \pm 0.10$	0.97	0.56	?	NM (45)
115	0.44	80.767404	33.470600	$2.90 \pm 0.24$	$0.56 \pm 0.09$	0.43	0.38	M	-
123	0.45	80.782318	33.467247	$3.77 \pm 0.27$	$0.49 \pm 0.06$	1.56	0.65	?	-
134	0.48	80.744271	33.400803	$3.19 \pm 0.21$	$0.57 \pm 0.08$	0.92	1.49	M	M(79)
139	0.40	80.723816	33.392075	$2.77 \pm 0.19$	$0.65 \pm 0.08$	0.57	0.10	$\mathbf{M}$	M(78)
140	0.41	80.719063	33.386875	$2.72 \pm 0.19$	$0.57 \pm 0.09$	0.75	0.67	$\mathbf{M}$	M(72)
141	0.42	80.717616	33.384277	$2.60 \pm 0.13$	$0.57 \pm 0.06$	0.67	0.80	M	M(78)
149	0.77	80.665351	33.371723	$2.81 \pm 0.07$	$0.56 \pm 0.03$	1.35	2.43	$\mathbf{M}$	M(80)
168	0.53	80.643091	33.489128	$2.34 \pm 0.20$	$0.60 \pm 0.10$	0.66	0.81	M	M(76)
196	$0.83^{*}$	80.788871	33.500652	$2.26 \pm 0.15$	$0.61 \pm 0.08$	0.73	1.21	?	M(79)
197	$0.20^{a}$	80.781174	33.497807	$2.19 \pm 0.13$	$0.57 \pm 0.06$	0.96	0.60	NM	NM(0)
199	0.73	80.781643	33.477089	$2.82 \pm 0.24$	$0.54 \pm 0.08$	2.19	0.98	?	-
209	$0.25^{*}$	80.823050	33.436195	$2.43 \pm 0.30$	$0.41 \pm 0.06$	1.50	0.46	NM	M(80)
213	$0.53^{*}$	80.798357	33.402302	$3.41 \pm 0.46$	$0.51 \pm 0.11$	0.84	1.45	?	NM (22)
215	0.47	80.789509	33.406975	$3.23 \pm 0.67$	$0.41 \pm 0.10$	0.40	0.97	$\mathbf{M}$	M (81)
219	0.48	80.782304	33.385307	$3.81 \pm 0.36$	$0.52\pm0.08$	1.11	0.78	$\mathbf{M}$	M(77)
222	0.39	80.770831	33.389034	$2.54 \pm 0.33$	$0.57 \pm 0.15$	0.21	1.16	$\mathbf{M}$	M (78)
228	0.40	80.741278	33.368721	$2.81 \pm 0.21$	$0.62 \pm 0.09$	1.17	0.66	$\mathbf{M}$	M(77)
301	0.39*	80.831142	33.452225	$3.21 \pm 0.07$	$0.55 \pm 0.03$	1.62	0.69	$\mathbf{M}$	M (78)
307	$0.42^{*}$	80.854608	33.435932	$3.44 \pm 0.10$	$0.57 \pm 0.04$	0.28	0.28	$\mathbf{M}$	M(79)
310	$0.20^{a}$	80.847118	33.419819	$2.15 \pm 0.30$	$0.45\pm0.07$	0.49	0.74	NM	M (84)
320	$0.46^{*}$	80.802256	33.366192	$2.81 \pm 0.17$	$0.55 \pm 0.08$	0.25	0.56	$\mathbf{M}$	M(65)
327	$0.20^{*}$	80.680573	33.288097	$1.16 \pm 0.14$	$0.50 \pm 0.13$	0.68	0.60	NM	M(75)
329	0.19*	80.656141	33.294849	$1.15 \pm 0.20$	$0.67 \pm 0.20$	1.22	0.83	NM	M (76)
355	$0.20^{a}$	80.899315	33.423325	$2.05 \pm 0.35$	$0.68 \pm 0.20$	0.09	0.53	NM	NM (48)
356	$0.20^{a}$	80.853457	33.408504	$2.59 \pm 0.36$	$0.57 \pm 0.16$	1.18	0.75	NM	-

 $<sup>^{\</sup>dagger} :$  Cuffey and Shapley (1937)

 $<sup>^{\</sup>ddagger}$ : To estimate E(B-V) values, UBV photometric data has been taken from Sharma et al. (2007)

<sup>\*:</sup> To estimate E(B-V) values, UBV photometric data has been taken from Massey et al. (1995)

 $<sup>^</sup>a$ : The foreground stars with  $E(B-V){=}0.20$  mag from ZAMS fitting  $^{\dagger\dagger}$ : Present Work

 $<sup>^{\</sup>dagger\dagger\dagger}$ : Dias et al. (2006)

Table 10. Mean values of  $P_V$  and  $\theta_V$  for members and non-members.

Cluster Id	$P_V \pm \sigma(\%)$	$\theta_V \pm \sigma(^{\circ})$	No of stars
	Members		
NGC 2281 NGC 1664 NGC 1960 Stock 8 NGC 1893	$0.9\pm0.2$ $1.4\pm0.2$ $1.2\pm0.1$ $2.5\pm0.2$ $2.8\pm0.4$	$17\pm6$ $172\pm4$ $160\pm3$ $161\pm4$ $160\pm4$	11 18 12 13 28
	Non-Members		
NGC 2281 NGC 1664 NGC 1960 Stock 8 NGC 1893	$0.9\pm0.3$ $2.5\pm0.9$ $1.2\pm0.4$ $1.8\pm0.3$ $1.6\pm0.4$	$14\pm 8$ $171\pm 14$ $155\pm 7$ $161\pm 3$ $166\pm 4$	3 9 3 6 11